

Coherent manipulation of graph states composed of finite-energy Gottesman-Kitaev-Preskill-encoded qubits

Kaushik P. Seshadreesan^{1,*}, Prajit Dhara^{1,2}, Ashlesha Patil¹, Liang Jiang³, and Saikat Guha¹

¹*College of Optical Sciences, University of Arizona, Tucson, Arizona 85721, USA*

²*Birla Institute of Technology & Science Pilani, Pilani, Rajasthan 333031, India and*

³*Pritzker School of Molecular Engineering, The University of Chicago*

Graph states are a central resource in measurement-based quantum information processing. In the photonic qubit architecture based on Gottesman-Kitaev-Preskill (GKP) encoding, the generation of high-fidelity graph states composed of realistic, finite-energy approximate GKP-encoded qubits thus constitutes a key task. We consider the finite-energy approximation of GKP qubit states given by a coherent superposition of shifted finite-squeezed vacuum states, where the displacements are Gaussian distributed. We present an exact description of graph states composed of such approximate GKP qubits as a coherent superposition of a Gaussian ensemble of randomly displaced ideal GKP-qubit graph states. We determine the transformation rules for the covariance matrix and the mean displacement vector of the Gaussian distribution of the ensemble under tools such as GKP-Steane error correction and fusion operations that can be used to grow large, high-fidelity GKP-qubit graph states. The former captures the noise in the graph state due to the finite-energy approximation of GKP qubits, while the latter relates to the possible absolute displacement shift errors on the individual qubits due to the homodyne measurements that are a part of these tools. The rules thus help in pinning down an exact coherent error model for graph states generated from truly finite-energy GKP qubits, which can shed light on their error correction properties.

I. INTRODUCTION

Photonic quantum technologies [1–3] provide a promising avenue for realizing quantum information processing in practice. A number of scalable architectures [4–7] for fault-tolerant universal quantum computation using realistically imperfect, noisy photonic elements, are being actively pursued experimentally [8–10]. Photonic, noisy intermediate-scale quantum (NISQ) processors are being utilized for demonstrations of quantum advantage over classical computations, e.g., in the boson sampling problem [11, 12]. Moreover, photonics is ubiquitously used in quantum communications [13] and quantum sensing [14] since photons form the most natural choice for carriers of quantum information.

Quantum information is most commonly encoded in the photonic domain in the discrete, finite degrees of freedom of single photons such as their polarization or propagation paths, or transverse spatial modes [15, 16], or frequency [17–19] or temporal modes [20, 21], or time bins [22, 23]. Deterministic generation of single photons forms the key challenge in realizing these encodings. Alternatively, encodings in the continuous, infinite quadrature degrees of freedom of spatial, frequency and temporal modes of the bosonic field have also been considered [24]. The class of Gaussian continuous variable (CV) states, such as the coherent states and squeezed states are easily generated using lasers and quantum nonlinear optics. CV quantum states are especially suited for the paradigm of measurement-based quantum computation since highly entangled CV multimode Gaussian

graph states [9, 10, 25] can be generated very efficiently. However, implementing universal quantum logic [26, 27], or any useful non-trivial quantum information processing task such as entanglement distillation [28] or quantum error correction [29] over CV states requires non-Gaussian elements such as photon number resolving detection or third or higher order optical nonlinearities [30].

In 2001, Gottesman, Kitaev and Preskill [31], introduced a hybrid encoding of quantum information in a bosonic mode, where an error-corrected qubit (more generally a qudit) is encoded in the continuous quadrature degrees of freedom of a bosonic mode. The GKP qubit, is protected against continuous, small displacement errors, which is critical to realize fault-tolerant quantum computation using CV quantum states and measurements. The resilience of GKP qubits against small displacement errors also makes them resistant to photon loss errors that are encountered in quantum communications. In fact, among all possible finite-dimensional subspace-encodings over the CV, infinite dimensional Hilbert space of a bosonic mode [32], the GKP qubit encoding is close to the optimal encoding for quantum capacity of Gaussian thermal loss channels with average photon number constraint [33]. This makes them suitable for error correction-based quantum repeaters [34, 35]. GKP qubit states are sufficiently non-Gaussian that all qubit-level Clifford operations can be deterministically and efficiently implemented using linear optics and coherent homodyne detection [36]. The key challenge in working with GKP qubits is that since they are ideal, unnormalized states, they can only be approximately realized in practice. There have been a few different proposals to realize approximate GKP qubit states and experimental implementations as well in recent works [37–41].

Given a supply of approximate GKP qubit states, the

* kaushiksesh@email.arizona.edu

generation of CV GKP graph states has important applications in measurement-based quantum computation as well as in all-optical quantum repeaters, where the graph states play the role of quantum memories [34, 42]. This task was investigated in Ref. [43]. However, the approximate GKP qubits were modeled as incoherent mixtures of ideal GKP qubits shifted by Gaussian distributed random displacements [44] that are strictly speaking still infinite energy states and hence unphysical. On the other hand, a coherent superposition of shifted finite-squeezed vacuum states, where the displacements are Gaussian distributed is a truly finite-energy approximation of a GKP qubit. An exact description of graph states based on such finite-energy, approximate GKP qubit pure states has been missing. This is accomplished in the present work. We start by considering the equivalent error wavefunction description of such finite-energy approximate GKP qubit pure states given by a coherent superposition of a Gaussian ensemble of ideal GKP-qubit states that are randomly displaced in phase space. Based on this, we represent a finite-energy GKP qubit graph state as a coherent superposition of a Gaussian ensemble of ideal GKP qubit graph states that are randomly displaced in phase space, characterized by the mean displacement vector and the covariance matrix of the Gaussian distribution for the random displacements. We derive the rules for the transformation of these characteristics under the GKP-Steane error correction protocol and graph fusion operations that are used to conditionally prepare large, high-fidelity graph states composed of individual GKP qubit pure states. An important merit of the description is that it provides a coherent error model for the GKP qubit graph states, which can be used to study their best error correction properties. These rules will thus be helpful in designing all-optical GKP-encoding-based quantum repeaters, and more generally for quantum computing with realistic, finite-energy, GKP qubit encoding. The paper is organized as follows. In Sec. II, we briefly review the GKP encoding of a qubit in a bosonic field mode along with its finite-energy approximations. In Sec. III, we describe finite-energy GKP graph states. In Sec. IV, we discuss an error correction procedure due to Steane [45], which is widely used for GKP qubits. In Sec. V, we discuss two fusion operations, that are used to merge two subgraphs or modify parts of a graph. In Sec. VI, we apply our description of finite-energy GKP qubit graph states to a graph state generation protocol to grow graph states. We illustrate how the description provides an accurate account of the noise and errors that build up in the graph state in the protocol.

II. GOTTESMAN-KITAEV-PRESKILL (GKP) QUBITS

Consider a bosonic mode described by its creation and annihilation operators \hat{a} and \hat{a}^\dagger , such that $[\hat{a}, \hat{a}^\dagger] = 1$. The corresponding Hermitian quadrature operators are

given by $\hat{q} = (\hat{a} + \hat{a}^\dagger)/\sqrt{2}$, $\hat{p} = (\hat{a} - \hat{a}^\dagger)/(\sqrt{2}i)$, where we have chosen $\hbar = 1$. The eigenstates of these operators are Fourier related as $|q\rangle = \frac{1}{\sqrt{2\pi}} \int dp \exp(ipq)|p\rangle$ and $|p\rangle = \frac{1}{\sqrt{2\pi}} \int dq \exp(-iqp)|q\rangle$. The symmetrically-ordered displacement operator for the mode is defined as

$$\hat{D}\left(\frac{u+iv}{\sqrt{2}}\right) = e^{-iu\hat{p}+iv\hat{q}}, \quad u, v \in \mathbb{R} \quad (1)$$

$$= e^{i\frac{uv}{2}} \hat{X}(u)\hat{Z}(v) = e^{-i\frac{uv}{2}} \hat{Z}(v)\hat{X}(u) \quad (2)$$

$$\text{where } \hat{Z}(v) = e^{iv\hat{q}}, \quad \hat{X}(u) = e^{-iu\hat{p}}. \quad (3)$$

The operators $\hat{X}(2\sqrt{\pi})$, $\hat{Z}(2\sqrt{\pi})$ commute, i.e., they can be simultaneously diagonalized. The ideal GKP qubit is defined as the 2-D subspace stabilized by these operators [31]. The logical bit-flip and phase flip operators for this qubit are defined as $\bar{X} = \hat{X}(\sqrt{\pi})$, $\bar{Z} = \hat{Z}(\sqrt{\pi})$. The ideal eigenstates of these operators form the bases for a GKP qubit and are given by

$$|\overline{\text{sign}(-1)^t}\rangle = \sum_{n=-\infty}^{+\infty} |(2n+t)\sqrt{\pi}\rangle_p, \quad t \in \{0, 1\} \quad (4)$$

$$|\bar{s}\rangle = \sum_{n=-\infty}^{+\infty} |(2n+s)\sqrt{\pi}\rangle_q, \quad s \in \{0, 1\}, \quad (5)$$

respectively. It can be easily shown using the Poisson summation formula that the states of (5) are uniform coherent superpositions of the states in (4) with appropriate phases, and vice versa. Moreover, the Wigner function of a uniform incoherent mixture of the bases states in (4) or (5), i.e., e.g., $(|\bar{0}\rangle\langle\bar{0}| + |\bar{1}\rangle\langle\bar{1}|)/2$, is a collection of delta function peaks that lie on a square lattice of spacing $\sqrt{\pi}$ in phase space. For this reason, the qubit that they define is referred to as a square-lattice GKP qubit.

Since the ideal square-lattice GKP qubit-basis states defined above are infinite superpositions of periodically displaced, infinite energy quadrature eigenstates, they are unnormalizable and unphysical. We can define finite-energy approximations of GKP qubit states as superpositions of periodically displaced, finitely squeezed vacuum states of variance $\sigma^2/2$ (where $\sigma^2 = 1$ corresponds to the vacuum), weighted by a Gaussian envelope function of variance $2/\sigma^2$, which therefore have finite energy, e.g.,

$$\begin{aligned} |\tilde{s}\rangle &\propto \sum_{n=-\infty}^{+\infty} e^{-\frac{\sigma^2((2n+s)\sqrt{\pi})^2}{2}} \hat{X}((2n+s)\sqrt{\pi}) \\ &\times \frac{1}{(\pi\sigma^2)^{1/4}} \int_{-\infty}^{+\infty} dq e^{-\frac{q^2}{2\sigma^2}} |0\rangle_q, \quad s \in \{0, 1\}, \end{aligned} \quad (6)$$

and likewise the $|\tilde{t}\rangle$ states. When $\sigma \ll \sqrt{\pi}$, the normalization constants of the above states are $\approx \sqrt{2\sigma}$.

When such a finitely squeezed approximate GKP qubit state, say the state $|\tilde{0}\rangle$ is measured along the q -quadrature using homodyne detection, the probability distribution of the outcomes and its approximation

when $\sigma \ll \sqrt{\pi}$ are given by

$$P_X(x) = |\langle x|\tilde{0}\rangle|^2 \approx \left| \sum_{n=-\infty}^{+\infty} \sqrt{2\sigma} e^{-\frac{\sigma^2(2n\sqrt{\pi})^2}{2}} \frac{e^{-\frac{(x-2n\sqrt{\pi})^2}{2\sigma^2}}}{(\pi\sigma^2)^{1/4}} \right|^2$$

$$\approx \sum_{n=-\infty}^{+\infty} (2\sigma) e^{-4\pi\sigma^2 n^2} \frac{e^{-\frac{(x-2n\sqrt{\pi})^2}{\sigma^2}}}{\sqrt{\pi\sigma^2}} \quad (7)$$

$$= \sum_{n=-\infty}^{+\infty} P_N[n] P_Q(x - 2\sqrt{\pi}n), \quad (8)$$

where

$$P_N[n] = (2\sigma) e^{-4\pi\sigma^2 n^2}, \quad n \in \mathbb{Z} \quad (9)$$

$$P_Q(q) = \frac{e^{-\frac{q^2}{\sigma^2}}}{\sqrt{\pi\sigma^2}}, \quad q \in \mathbb{R} \quad (10)$$

are Gaussian distributions of an integer-valued random variable N and a real-valued random variable Q , respectively. We denote these random variables and their distributions by the following shorthand notation that highlights the distribution (along with the field), and the mean and variance: $N \sim \mathcal{G}_{\mathbb{Z}}(0, 1/(8\pi\sigma^2))$ and $Q \sim \mathcal{G}_{\mathbb{R}}(0, \sigma^2/2)$, where $\sigma^2 \in \mathbb{R}$. Rescaling the random variable N by $2\sqrt{\pi}$, we have a real-valued random variable $2\sqrt{\pi}N \sim \mathcal{G}_{\mathbb{R}}(0, 1/(2\sigma^2))$. Thus, the outcome X is a random variable given by

$$X = 2\sqrt{\pi}N + Q, \quad (11)$$

whose distribution $P_X(x)$, $x \in \mathbb{R}$ is given by the convolution of the distributions of $2\sqrt{\pi}N$ and Q . Likewise, when a coherent superposition state of the form $(|\tilde{0}\rangle + |\tilde{1}\rangle)/\sqrt{2}$ is measured with q -homodyne detection, we have

$$P_X(x) = \frac{1}{2} |\langle x|\tilde{0}\rangle + \langle x|\tilde{1}\rangle|^2$$

$$\approx \frac{1}{2} \left| \sum_{n=-\infty}^{+\infty} \sqrt{2\sigma} e^{-\frac{\sigma^2(2n\sqrt{\pi})^2}{2}} \frac{e^{-\frac{(x-2n\sqrt{\pi})^2}{2\sigma^2}}}{(\pi\sigma^2)^{1/4}} + \sum_{n'=-\infty}^{+\infty} \sqrt{2\sigma} e^{-\frac{\sigma^2((2n'+1)\sqrt{\pi})^2}{2}} \frac{e^{-\frac{(x-(2n'+1)\sqrt{\pi})^2}{2\sigma^2}}}{(\pi\sigma^2)^{1/4}} \right|^2 \quad (12)$$

$$= \frac{1}{2} \left| \sum_{n=-\infty}^{+\infty} \sqrt{2\sigma} e^{-\frac{\sigma^2(n\sqrt{\pi})^2}{2}} \frac{e^{-\frac{(x-n\sqrt{\pi})^2}{2\sigma^2}}}{(\pi\sigma^2)^{1/4}} \right|^2 \quad (13)$$

$$\approx \sum_{n=-\infty}^{+\infty} \sigma e^{-\pi\sigma^2 n^2} \frac{e^{-\frac{(x-n\sqrt{\pi})^2}{\sigma^2}}}{\sqrt{\pi\sigma^2}} \quad (14)$$

$$= \sum_{n=-\infty}^{+\infty} P_N[n] P_Q(x - \sqrt{\pi}n), \quad (15)$$

where

$$P_N[n] = \sigma e^{-\pi\sigma^2 n^2}, \quad n \in \mathbb{Z} \quad (16)$$

$$P_Q(q) = \frac{e^{-\frac{q^2}{\sigma^2}}}{\sqrt{\pi\sigma^2}}, \quad q \in \mathbb{R} \quad (17)$$

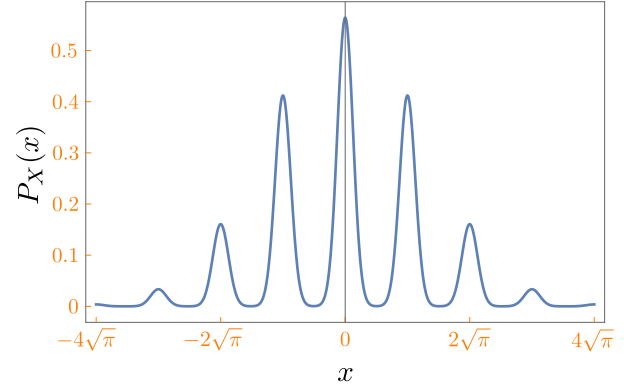


Figure 1. Probability distribution of outcomes from q -quadrature measurement of a finite-energy GKP qubit $(|\tilde{0}\rangle + |\tilde{1}\rangle)/\sqrt{2}$ for a squeezing value of 10 dB.

are Gaussian distributions of an integer-valued random variable $N \sim \mathcal{G}_{\mathbb{Z}}(0, 1/(2\pi\sigma^2))$ and a real-valued random variable $Q \sim \mathcal{G}_{\mathbb{R}}(0, \sigma^2/2)$, respectively. That is, the outcome is a random variable

$$X = \sqrt{\pi}N + Q, \quad (18)$$

whose distribution $P_X(x)$, $x \in \mathbb{R}$ is the convolution of distributions of $\sqrt{\pi}N \sim \mathcal{G}_{\mathbb{R}}(0, 1/(2\sigma^2))$ and $Q \sim \mathcal{G}_{\mathbb{R}}(0, \sigma^2/2)$. Figure 1 plots this outcome distribution for the case where the constituent squeezed vacuum states (in the weighted superposition) are 10 dB squeezed below vacuum variance in the q -quadrature, i.e., where the $|\tilde{0}\rangle$, $|\tilde{1}\rangle$, in the superposition are of the form in (6) with $\sigma^2 = 0.1$ (where squeezing in dB is calculated as $-10 \log_{10} \sigma^2$). Note that in the above descriptions of finite-energy GKP qubit states, it is implicit that the conjugate quadrature is correspondingly anti-squeezed with a variance equalling that of the Gaussian outer envelope. More generally, the outer Gaussian envelope of a finite-energy GKP qubit state can have a variance $\leq 1/(2\sigma^2)$, so that the squeezing-anti-squeezing product is $\leq 1/4$ [46].

An equivalent, more general description of an arbitrary finite-energy GKP qubit state $|\tilde{\psi}\rangle$ in terms of the corresponding ideal GKP qubit state $|\psi\rangle$ (up to normalization) that was also discussed in Ref. [31] is given by

$$|\tilde{\psi}\rangle = \int du dv \eta(u, v) e^{i(-u\hat{p}+v\hat{q})} |\psi\rangle, \quad (19)$$

$$= \int du dv \eta(u, v) e^{\frac{iuv}{2}} e^{-iu\hat{p}} e^{iv\hat{q}} |\psi\rangle, \quad (20)$$

$$\eta(u, v) = \frac{1}{\sqrt{\pi\kappa\delta}} e^{-\frac{1}{2}(\frac{(u-u')^2}{\delta^2} + \frac{(v-v')^2}{\kappa^2})}; \quad 0 < \delta\kappa < 1, \quad (21)$$

where $\eta(u, v)$ is the square root of a real-valued, characteristic bivariate Gaussian distribution for the state, known as its error wavefunction, where (u', v') and (δ^2, κ^2) are the means and variances of the (q, p) -quadrature displacements, respectively. The state

$|\tilde{\psi}\rangle$ is thus a coherent superposition of displaced ideal GKP qubit states, where the displacements are drawn from the distribution $|\eta(u, v)|^2$, which effectively introduces a Gaussian envelope. For the explicit equivalence of the error wavefunction description to the quadrature basis description, see Appendix A. Note that a superposition of displacements is different from an incoherent mixture of displacements, which characterize thermal noise.

III. GRAPH STATES COMPOSED OF FINITE SQUEEZED GKP QUBITS

Consider a finite, simple, undirected graph $G(\mathcal{V}, \mathcal{E})$, where \mathcal{V} is the set of vertices v_i with cardinality $|\mathcal{V}| = n$, and \mathcal{E} is the set of edges $e_{ij} = (v_i, v_j)$ connecting vertices v_i, v_j . A graph state $|G\rangle$ is defined as

$$|\overline{\Psi}_G\rangle = \prod_{e \in \mathcal{E}} C_{Ze} |\overline{\psi}\rangle^{\otimes n}, \quad (22)$$

where the vertices in \mathcal{V} of graph G have been associated with qubits in the $|\overline{\psi}\rangle$ state and the edges $e \in \mathcal{E}$ with the controlled-phase gate denoted by C_Z .

When the vertices are bosonic modes initialized as finite-energy approximate GKP qubits of the form in (19-21), where $\delta_i^2 = l_i \sigma^2$, $\kappa_i^2 = m_i \sigma^2$ and $u'_i = \mu_{q_i}$, $v'_i = \mu_{p_i}$, $\forall i \in \{v_1, \dots, v_n\}$, σ^2 is some unit variance and all $l_i, m_i, \mu_{q_i}, \mu_{p_i} \in \mathbb{R}$, the corresponding graph state takes the form

$$|\overline{\Psi}_G\rangle = \int d\vec{x} \eta_G(\vec{\mu}, V, \vec{x}) \prod_{i=1}^n e^{\frac{i x_i x_{n+i}}{2}} e^{-i x_i \hat{p}_i} e^{i x_{n+i} \hat{q}_i} |\overline{\Psi}_G\rangle. \quad (23)$$

Here $|\overline{\Psi}_G\rangle$ denotes the ideal GKP-qubit graph state of the form in (22) associated with the graph $G(\mathcal{V}, \mathcal{E})$, which is obtained using the continuous variable controlled-phase gate that is the quadratic Gaussian unitary given by $C_{Ze} = e^{-i \hat{q}_{v_i} \hat{q}_{v_j}}$ acting on edges $e_{ij} = (v_i, v_j)$, where the vertices are associated with the ideal $|\overline{\psi}\rangle$ GKP qubit state of (4). In the Heisenberg picture, the C_Z unitary transforms the quadrature operators of two modes v_1, v_2 symmetrically as

$$\begin{aligned} C_Z^\dagger \hat{q}_{v_1} C_Z &= \hat{q}_{v_1} \\ C_Z^\dagger \hat{p}_{v_1} C_Z &= \hat{p}_{v_1} - \hat{q}_{v_2} \\ C_Z^\dagger \hat{q}_{v_2} C_Z &= \hat{q}_{v_2} \\ C_Z^\dagger \hat{p}_{v_2} C_Z &= \hat{p}_{v_2} - \hat{q}_{v_1}. \end{aligned} \quad (24)$$

The corresponding error wavefunction $\eta_G(\vec{\mu}, V, \vec{x})$ is the square root of the $2n$ -variate Gaussian distribution of the now correlated coherent random displacements acting on the underlying ideal GKP qubits, given by

$$\eta_G(V, \vec{\mu}, \vec{x}) = \frac{e^{-\frac{1}{2}((\vec{x}-\vec{\mu}) \cdot V^{-1} \cdot (\vec{x}-\vec{\mu})^T)}}{(\pi^{2n} \det(V))^{1/4}}, \quad (25)$$

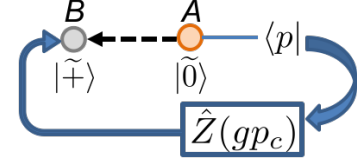


Figure 2. A schematic of the Steane error correction procedure for reducing the noise variance along the p -quadrature in an approximate GKP qubit using an approximate GKP ancilla qubit. The black dashed arrow indicates a Controlled-Not gate.

where

$$\vec{x} = (s_1, s_2, \dots, s_n, t_1, t_2, \dots, t_n), \quad (26)$$

$$\vec{\mu} = \{\mu'_q, \mu'_p\}, \quad (27)$$

$$\vec{\mu}'_q \equiv \{\mu_{q_i}\}_{i=1}^n \quad (28)$$

$$\vec{\mu}'_p \equiv \{\mu_{p_i}\}_{i=1}^n, \quad \mu_{p_i} = \mu_{p_i} - \sum_j A_{ij} \mu_{q_j}, \quad (29)$$

$$V = \begin{pmatrix} Q_{n \times n} & R_{n \times n}^T \\ R_{n \times n} & P_{n \times n} \end{pmatrix} \sigma^2, \quad (30)$$

$$Q = \text{diag}(\vec{l}), \quad \vec{l} \equiv \{l_i\}_{i=1}^n, \quad (31)$$

$$P = \text{diag}(\vec{p}), \quad \vec{p} \equiv \{p_i\}_{i=1}^n, \quad p_i = m_i + \sum_j A_{ij} l_j, \quad (32)$$

$$R \equiv \{R_{ij}\}_{i,j=1}^n, \quad R_{ij} = -A_{ij} l_j, \quad (33)$$

and A is the adjacency matrix of graph $G(\mathcal{V}, \mathcal{E})$. The above form for η_G is the result of the action of the affine-symplectic map corresponding to the CV C_Z unitary operation on the quadrature variables in phase space [24]. The graph state of (23) most generally can thus be compactly represented by a node-weighted version of the graph $G(\mathcal{V}, \mathcal{E})$, the node weights being the mean quadrature displacements of the modes $\vec{\mu} = (\vec{\mu}'_q, \vec{\mu}'_p)$, and in addition by specifying a $2n \times 2n$, real, symmetric covariance matrix V associated with the correlated coherent random displacements \vec{s}, \vec{t} acting on the underlying ideal GKP qubit graph state. In other words, we can represent $|\overline{\Psi}_G\rangle \equiv G(\mathcal{V}, \mathcal{E}, \vec{\mu}_q, \vec{\mu}_p, V)$.

Evidently, if large graph states are generated from individual finite-energy approximate GKP qubits using C_Z gates along, then the p -quadrature variances of the modes can quickly accumulate, rendering the state too noisy. The next two sections discuss tools that help remedy this situation.

IV. GKP ERROR CORRECTION OF FINITE SQUEEZED GKP QUBIT GRAPH STATES

The GKP Steane error correction is a procedure that helps reduce quadrature noise in the finite squeezed GKP qubits at the cost of a possible mean displacement error. We will begin by describing the action of the procedure on a trivial single mode graph state, i.e., a single

approximate GKP qubit state of the form in (19), and then generalize the results to a vertex of a larger graph. The procedure involves a unitary interaction between the “data” qubit, whose noise along p or q quadrature is desired to be reduced, and an ancilla that is also prepared in a finite-energy approximation of an eigenstate of the conjugate quadrature, but with presumably lower noise variance than the data qubit in the quadrature of interest. We note that Steane error correction for the case of a single qubit graph has been previously discussed in [47].

We discuss GKP-Steane error correction for p -quadrature noise reduction here. A schematic of the procedure is shown in Figure 2. It consists of preparing an ancilla GKP qubit (qubit A) in the $|\tilde{0}\rangle$ state of (5) and performing the CV Controlled-NOT gate C_X with the ancilla qubit as the control and the data qubit (qubit B) as the target. This is followed by performing a p -quadrature homodyne measurement on the ancilla and a feedback $\hat{Z}(gy)$ displacement on the data GKP qubit, where y is the measurement outcome and g is a suitable gain factor. In this work, the feedback displacement is chosen such that it removes the measurement outcome-dependent component of the conditional mean displacement on the data qubit(s). The C_X gate in CV is given by the unitary interaction $C_X^{C \rightarrow T} = e^{-i\hat{q}_C \hat{p}_T}$, where C, T denote the control and target modes, respectively. The CV C_X gate can be implemented using beam splitters and inline single-mode squeezers as described later in Sec. V.

Note that the procedure for q -quadrature noise reduction would similarly involve an ancilla prepared in a $|\tilde{+}\rangle$ and the C_X between the data and the ancilla qubits, but with the data qubit as the control and the ancilla qubit as the target. This is followed by a q -quadrature measurement of the ancilla qubit and a feedback measurement on the data qubit.

A. p -Steane error correction of a single finite-energy GKP qubit

In p -quadrature GKP Steane error correction of a single finite-energy GKP qubit in a state of the form in (19), the interaction between the data and ancilla approximate GKP qubits results in a two-mode state given by

$$\begin{aligned} |\psi\rangle_{AB} &= C_X^{A \rightarrow B} |\tilde{0}\rangle_A \otimes |\tilde{+}\rangle_B \\ &= \int du_A dv_A \eta_A(u_A, v_A) \int du_B dv_B \eta_B(u_B, v_B) \\ &\times C_X^{A \rightarrow B} e^{i(-u_A \hat{p}_A + v_A \hat{q}_A)} e^{i(-u_B \hat{p}_B + v_B \hat{q}_B)} |\tilde{0}\rangle_A |\tilde{+}\rangle_B \quad (34) \\ &= \int ds_A dt_A ds_B dt_B \eta_{AB}(s_A, s_B, t_A, t_B) \\ &\times e^{i(-s_A \hat{p}_A + t_A \hat{q}_A)} e^{i(-s_B \hat{p}_B + t_B \hat{q}_B)} |\tilde{0}\rangle_A |\tilde{+}\rangle_B, \quad (35) \end{aligned}$$

where $s_A = u_A$, $s_B = u_B + u_A$, $t_A = v_A - v_B$, $t_B = v_B$ and $\eta_{AB}(s_A, s_B, t_A, t_B)$ is the square root of a 4-variate

Gaussian distribution

$$\eta_{AB}(s_A, s_B, t_A, t_B) = \frac{e^{-\frac{1}{2}(\vec{x}V^{-1}\vec{x}^T)}}{\pi(\det(V))^{1/4}}, \quad (36)$$

with

$$\vec{x} = (s_A, s_B, t_A, t_B), \quad (37)$$

$$V = V_s \oplus V_t, \quad (38)$$

$$V_s = \begin{pmatrix} l_A & l_A \\ l_A & l_B + l_A \end{pmatrix} \sigma^2, \quad V_t = \begin{pmatrix} m_A + m_B & -m_B \\ -m_B & m_B \end{pmatrix} \sigma^2 \quad (39)$$

We note that $C_X^{A \rightarrow B} |\tilde{0}\rangle_A \otimes |\tilde{+}\rangle_B = |\tilde{0}\rangle_A \otimes |\tilde{+}\rangle_B$.

The state $|\psi\rangle_{AB}$ can be equivalently written as

$$\begin{aligned} &\int ds_A ds_B \chi_{AB}(s_A, s_B) \int dt_A dt_B \mathcal{P}(t_A) \mathcal{Q}(t_B | t_A) \\ &\times e^{i(-s_A \hat{p}_A + t_A \hat{q}_A)} e^{i(-s_B \hat{p}_B + t_B \hat{q}_B)} |\tilde{0}\rangle_A |\tilde{+}\rangle_B, \quad (40) \end{aligned}$$

where $\chi_{AB}(s_A, s_B)$, and $\{\mathcal{P}(t_A), \mathcal{Q}(t_B | t_A)\}$ are the square roots of bivariate and univariate, real-valued Gaussian distributions, respectively, denoted as

$$\chi_{AB}(s_A, s_B) \sim \mathcal{G}_{\mathbb{R}}^{1/2}((0, 0), V_s), \quad (41)$$

$$\mathcal{P}(t_A) \sim \mathcal{G}_{\mathbb{R}}^{1/2}(0, (m_A + m_B)\sigma^2), \quad (42)$$

$$\mathcal{Q}(t_B | t_A) \sim \mathcal{G}_{\mathbb{R}}^{1/2}\left(\frac{-m_B}{m_A + m_B} t_A, \frac{m_A m_B}{m_A + m_B} \sigma^2\right). \quad (43)$$

The latter follows by applying Bayes' rule.

Ancilla measurement and conditional post-measurement state

When qubit A is measured over its p -quadrature, we get an outcome $y \in \mathbb{R}$ with probability $P_Y(y)$ and a conditional state $|\phi\rangle_{B|y}$ on qubit B , that can be deduced from the conditional unnormalized state given by (see Appendix B for the derivation)

$$\begin{aligned} p\langle y|_A \cdot |\psi\rangle_{AB} &= \sqrt{P_Y(y)} |\phi\rangle_{B|y} \\ &= 2\sqrt{\pi} \sum_n \frac{e^{-\frac{(y-n\sqrt{\pi})^2}{2(m_A+m_B)\sigma^2}}}{(\pi(m_A+m_B)\sigma^2)^{1/4}} \frac{e^{-\frac{(y+n\sqrt{\pi})^2}{8\frac{(l_A+l_B)}{l_A l_B} \sigma^2}}}{(4\pi\frac{(l_A+l_B)}{l_A l_B} \sigma^2)^{1/4}} \\ &\times \left(\int ds_B dt_B \frac{e^{-\frac{s_B^2}{2(l_A+l_B)\sigma^2}}}{(\pi(l_A+l_B)\sigma^2)^{1/4}} \frac{e^{-\frac{(t_B + \frac{m_B}{m_A+m_B}(y-n\sqrt{\pi}))^2}{2\frac{m_A m_B}{m_A+m_B} \sigma^2}}}{(\pi\frac{m_A m_B}{m_A+m_B} \sigma^2)^{1/4}} \right. \\ &\left. e^{-i\frac{l_A}{2(l_A+l_B)}(y+n\sqrt{\pi})s_B} e^{i(-s_B \hat{p}_B + t_B \hat{q}_B)} |\tilde{+}\rangle_B \right) \quad (44) \end{aligned}$$

Assuming $\sqrt{(m_A + m_B)\sigma} \ll \sqrt{\pi}/2$, the support of $P_Y(y)$ is mainly concentrated around $y = n\sqrt{\pi}$, $n \in \mathbb{Z}$. When

$y - n\sqrt{\pi}$ is small for some $n \in \mathbb{Z}$, then $y + n\sqrt{\pi} \approx 2n\sqrt{\pi}$ for that n , i.e., $\sqrt{P_Y(y)}|\phi\rangle_{B|y}$

$$\propto \sum_n \frac{e^{-\frac{(2n\sqrt{\pi})^2}{8\frac{(l_A+l_B)}{l_A l_B \sigma^2}}}}{e^{-\frac{(y-n\sqrt{\pi})^2}{2(m_A+m_B)\sigma^2}}} \frac{1}{(4\pi\frac{(l_A+l_B)}{l_A l_B \sigma^2})^{1/4} (\pi(m_A+m_B)\sigma^2)^{1/4}} \\ \left(\int ds_B dt_B \frac{e^{-\frac{s_B^2}{2(l_A+l_B)\sigma^2}}}{e^{-\frac{(t_B+\frac{m_B}{m_A+m_B}(y-n\sqrt{\pi}))^2}{2\frac{m_A m_B}{m_A+m_B}\sigma^2}}} \frac{1}{(\pi(l_A+l_B)\sigma^2)^{1/4} (\pi\frac{m_A m_B}{m_A+m_B}\sigma^2)^{1/4}} \right. \\ \left. e^{-i\frac{l_A}{l_A+l_B}n\sqrt{\pi}s_B} e^{i(-s_B\hat{p}_B+t_B\hat{q}_B)} |\bar{+}\rangle_B \right). \quad (45)$$

Moreover, $P_Y(y)$ can be approximated as

$$\propto \sum_n \left| \frac{e^{-\frac{(n\sqrt{\pi})^2}{2\frac{(l_A+l_B)}{l_A l_B \sigma^2}}}}{e^{-\frac{(y-n\sqrt{\pi})^2}{2(m_A+m_B)\sigma^2}}} \frac{1}{(\pi\frac{(l_A+l_B)}{l_A l_B \sigma^2})^{1/4} (\pi(m_A+m_B)\sigma^2)^{1/4}} \right|^2 \quad (46)$$

$$= \sum_n \frac{e^{-\frac{(n\sqrt{\pi})^2}{2\frac{(l_A+l_B)}{l_A l_B \sigma^2}}}}{e^{-\frac{(y-n\sqrt{\pi})^2}{2(m_A+m_B)\sigma^2}}} \frac{1}{(\pi\frac{(l_A+l_B)}{l_A l_B \sigma^2})^{1/2} (\pi(m_A+m_B)\sigma^2)^{1/2}} \quad (47)$$

$$= \sum_n P_N[n] P_Q(y - n\sqrt{\pi}), \quad (48)$$

where the random variables N and Q are given by

$$N \sim \mathcal{G}_{\mathbb{Z}}(0, \left(\frac{l_A+l_B}{l_A l_B}\right)/(2\pi\sigma^2)), \quad n \in \mathbb{Z}, \quad (49)$$

$$Q \sim \mathcal{G}_{\mathbb{R}}(0, (m_A+m_B)\sigma^2/2), \quad p \in \mathbb{R}. \quad (50)$$

That is, the outcome of the p -homodyne measurement of qubit A is

$$y = \sqrt{\pi}N + Q, \quad (51)$$

and its distribution is given by the convolution of $N\sqrt{\pi} \sim \mathcal{G}_{\mathbb{R}}(0, \left(\frac{l_A+l_B}{l_A l_B}\right)/(2\sigma^2))$, $n \in \mathbb{Z}$ and Q . Note that Q has the same distribution as t_A .

Thus, the conditional post-measurement state of qubit B can be written as

$$|\phi\rangle_{B|y} = \frac{1}{\sqrt{\mathcal{N}}} \sum_n \sqrt{P_N[n] P_Q(y - n\sqrt{\pi})} \int ds_B dt_B \\ \zeta(s_B, t_B) e^{-i\frac{l_A}{l_A+l_B}n\sqrt{\pi}s_B} e^{i(-s_B\hat{p}_B+t_B\hat{q}_B)} |\bar{+}\rangle_B, \quad (52)$$

$$\zeta(s_B, t_B) = \frac{e^{-\frac{s_B^2}{2(l_A+l_B)\sigma^2}}}{e^{-\frac{(t_B+\frac{m_B}{m_A+m_B}(y-n\sqrt{\pi}))^2}{2\frac{m_A m_B}{m_A+m_B}\sigma^2}}} \frac{1}{(\pi(l_A+l_B)\sigma^2)^{1/4} (\pi\frac{m_A m_B}{m_A+m_B}\sigma^2)^{1/4}}, \quad (53)$$

$$\mathcal{N} = \sum_n P_N[n] P_Q(y - n\sqrt{\pi}). \quad (54)$$

By a change of variables $t_B \rightarrow t_B - \frac{m_B}{m_A+m_B}(y - n\sqrt{\pi})$, the above state can be equivalently written as

$$|\phi\rangle_{B|y} = \frac{1}{\sqrt{\mathcal{N}}} \sum_n \sqrt{P_N[n] P_Q(y - n\sqrt{\pi})} \\ \int ds_B dt_B \zeta(s_B, t_B) e^{-i\frac{l_A}{l_A+l_B}n\sqrt{\pi}s_B} \\ e^{i(-s_B\hat{p}_B + (t_B - \frac{m_B}{m_A+m_B}(y-n\sqrt{\pi}))\hat{q}_B)} |\bar{+}\rangle_B, \quad (55)$$

$$\zeta(s_B, t_B) = \frac{e^{-\frac{s_B^2}{2(l_A+l_B)\sigma^2}}}{e^{-\frac{(t_B - \frac{m_B}{m_A+m_B}(y-n\sqrt{\pi}))^2}{2\frac{m_A m_B}{m_A+m_B}\sigma^2}}} \frac{1}{(\pi(l_A+l_B)\sigma^2)^{1/4} (\pi\frac{m_A m_B}{m_A+m_B}\sigma^2)^{1/4}}, \quad (56)$$

where \mathcal{N} is the normalization factor of (54) and the mean displacement has been moved to the displacement operator from the error wavefunction.

Feedback displacement on B

Following the ancilla measurement, a feedback displacement $\hat{Z}(gp_c(y))$, y being the ancilla measurement outcome and g being a gain factor, is applied on mode B . The quantity $p_c(y)$ is chosen to the amount of

$$p_c(y) = y \mod \sqrt{\pi} \quad (57)$$

such that $p_c(y) \in [-\sqrt{\pi}/2, \sqrt{\pi}/2]$. That is, e.g.,

$$0 < y < \frac{\sqrt{\pi}}{2} \Rightarrow p_c(y) = y \quad (58)$$

$$\frac{\sqrt{\pi}}{2} < y < \sqrt{\pi} \Rightarrow p_c(y) = y - \sqrt{\pi}. \quad (59)$$

More generally, for $y > 0$ and $n' = \lfloor \frac{y}{\sqrt{\pi}} \rfloor \in \mathbb{Z}$, we have $p_c(y)$

$$= \begin{cases} y - n'\sqrt{\pi}, & y - n'\sqrt{\pi} < \sqrt{\pi}/2 \\ y - (n'+1)\sqrt{\pi}, & \sqrt{\pi} > y - n'\sqrt{\pi} > \sqrt{\pi}/2 \end{cases} \quad (60)$$

Likewise, for $y < 0$ and $n' = \lfloor \frac{|y|}{\sqrt{\pi}} \rfloor \in \mathbb{Z}$, we have $p_c(y)$

$$= \begin{cases} y + n'\sqrt{\pi}, & |y| - n'\sqrt{\pi} < \sqrt{\pi}/2 \\ y + (n'+1)\sqrt{\pi}, & \sqrt{\pi} > |y| - n'\sqrt{\pi} > \sqrt{\pi}/2 \end{cases} \quad (61)$$

When the gain factor is chosen to be $g = \frac{m_B}{m_A+m_B}$, for an ancilla measurement outcome in the interval of $0 < y < \frac{\sqrt{\pi}}{2}$, the state of qubit B is transformed as $|\phi\rangle_{B|y} \rightarrow |\psi\rangle_{B|y}$, where $|\psi\rangle_{B|y}$

$$= \hat{Z}\left(\frac{m_B}{m_A+m_B}p_c(y)\right) |\phi\rangle_{B|y} \\ = \frac{1}{\sqrt{\mathcal{N}}} \sum_n \sqrt{P_N[n] P_Q(y - n\sqrt{\pi})} \\ \int ds_B dt_B \zeta(s_B, t_B) e^{is_B\left(\frac{m_B}{m_A+m_B}\frac{y}{2} - \frac{l_A}{l_A+l_B}n\sqrt{\pi}\right)} \\ e^{i(-s_B\hat{p}_B + (t_B + \frac{m_B}{m_A+m_B}n\sqrt{\pi})\hat{q}_B)} |\bar{+}\rangle_B, \quad (62)$$

\mathcal{N} being the normalization factor of (54). Note that with this choice of g , we get rid of the y -dependent mean displacement. On the contrary, there is now a y -dependent phase factor, which is arrived at by carefully manipulating the joint displacement operator with the \hat{Z} displacement from the feedback using the decompositions in (2). However, this phase is inconsequential since it is a global phase, present in all terms in the coherent superposition. When $m_A \ll m_B$, we have $|\psi\rangle_{B|y}$

$$\approx \frac{1}{\sqrt{\mathcal{N}}} \sum_n \sqrt{P_N[n]P_Q(y - n\sqrt{\pi})} \int ds_B dt_B \xi(s_B, t_B) e^{is_B \left(\frac{y}{2} - \frac{l_A}{l_A + l_B} n\sqrt{\pi}\right)} e^{i(-s_B \hat{p}_B + (t_B + n\sqrt{\pi}) \hat{q}_B)} |\bar{+}\rangle_B, \quad (63)$$

where

$$\begin{aligned} \xi(s_B, t_B) &= \lim_{m_A/m_B \rightarrow 0} \zeta(s_B, t_B) \\ &= \frac{e^{-\frac{s_B^2}{2(l_A + l_B)\sigma^2}}}{(\pi(l_A + l_B)\sigma^2)^{1/4}} \frac{e^{-\frac{t_B^2}{2m_A\sigma^2}}}{(\pi m_A \sigma^2)^{1/4}}. \end{aligned} \quad (64)$$

More generally, when $m_A \ll m_B$, for any $y \geq 0$, we have $|\psi\rangle_{B|y} \approx$

$$\frac{1}{\sqrt{\mathcal{N}}} \sum_n \sqrt{P_N[n]P_Q(y - n\sqrt{\pi})} \int ds_B dt_B \xi(s_B, t_B) e^{is_B \left(\frac{y \mp z\sqrt{\pi}}{2} - \frac{l_A}{l_A + l_B} n\sqrt{\pi}\right)} e^{i(-s_B \hat{p}_B + (t_B + (n \mp z)\sqrt{\pi}) \hat{q}_B)} |\bar{+}\rangle_B, \quad (65)$$

$$z = \begin{cases} n', & |y| - n'\sqrt{\pi} < \sqrt{\pi}/2 \\ (n' + 1), & \sqrt{\pi} > |y| - n'\sqrt{\pi} > \sqrt{\pi}/2 \end{cases}, \quad (66)$$

$$n' = \lfloor \frac{|y|}{\sqrt{\pi}} \rfloor \in \mathbb{Z}, \quad (67)$$

where $\xi(s_B, t_B)$ is as given in (64).

Mean displacement error in the Steane error-corrected state

We will now focus on the interval $|y| < \sqrt{\pi}$ for the ancilla measurement outcome. Once again, assuming $\sqrt{(m_A + m_B)\sigma} \ll \sqrt{\pi}/2$, the probability $P_Y(y)$ of (48) for outcome y can be approximated as

$$P_Y(y) \approx P_N[0]P_Q(y) + P_N[1]P_Q(\sqrt{\pi} - |y|). \quad (68)$$

Further, when $|y| \leq \sqrt{\pi}/2$ and $m_A \ll m_B$, the error-corrected state can be approximated as $|\psi\rangle_{B|y} \approx$

$$\frac{\sqrt{P_N[0]P_Q(|y|)}|\psi_0\rangle + \sqrt{P_N[1]P_Q(\sqrt{\pi} - |y|)}|\psi_1\rangle}{\sqrt{P_Y(y)}}, \quad (69)$$

where

$$\begin{aligned} |\psi_0\rangle &= \int ds_B dt_B \xi(s_B, t_B) e^{i(-s_B \hat{p}_B + t_B \hat{q}_B)} |\bar{+}\rangle_B, \quad (70) \\ |\psi_1\rangle &= \int ds_B dt_B \xi(s_B, t_B) e^{i(-s_B \hat{p}_B + (t_B - \sqrt{\pi}) \hat{q}_B)} |\bar{+}\rangle_B, \\ &= \int ds_B dt_B \xi(s_B, t_B + \sqrt{\pi}) e^{i(-s_B \hat{p}_B + t_B \hat{q}_B)} |\bar{+}\rangle_B, \end{aligned} \quad (71)$$

and $P_Y(y)$ and $\xi(s_B, t_B)$ are as given in (68) and (64), respectively. Note that we are ignoring phase factors in the above expressions since they do not affect the mean displacement error probabilities discussed below.

We observe that the p -displacements in $|\psi_1\rangle$ have an additional mean shift of $\sqrt{\pi}$, i.e., an offset of half the GKP grid spacing relative to $|\psi_0\rangle$. Since the underlying ideal GKP qubit state in both $|\psi_0\rangle$ and $|\psi_1\rangle$ is an eigenstate of the \hat{X} operator (the $|\bar{+}\rangle$ state), the additional mean p -displacement of $\sqrt{\pi}$ in $|\psi_1\rangle$ implies a logical Z -flip of the underlying ideal GKP qubit state. In other words, the $|\psi_1\rangle$ has an orthogonal support compared to $|\psi_0\rangle$ in the GKP grid state basis.

However, it should be noted that $|\psi_1\rangle$ is not exactly the zero mean finite squeezed $|\bar{-}\rangle$, because it has its Gaussian envelope offset relative to that state. The p -quadrature wavefunction of the state (and more generally for states corresponding to shifted-mean error wavefunctions) is derived in Appendix C. Figure 3 plots the p -quadrature wavefunction of $|\psi_1\rangle$ at the output of the p -quadrature Steane error correction when starting with an input-ancilla error wavefunction covariance matrix of the form in (39) with $l_A = m_A = l_B = 1, m_B \gg 1$ and $\sigma^2 = 0.1$ (corresponding to 10 dB vacuum squeezing along the p -quadrature). This output $|\psi_1\rangle$ has its error wavefunction covariance matrix specified by $\delta^2 = 2\sigma^2, \kappa^2 = \sigma^2$. Figure 3 also contrasts the plot of $|\psi_1\rangle$ with that of the $|\bar{-}\rangle$ corresponding to the same error wavefunction covariance matrix state. Since $|y| \leq \sqrt{\pi}/2$, we have $P_N[0]P_Q(|y|) > P_N[1]P_Q(\sqrt{\pi} - |y|)$, which implies a higher weight for $|\psi_0\rangle$ in the superposition.

On the other hand, when $\sqrt{\pi} > |y| > \sqrt{\pi}/2$ and $m_A \ll m_B$, we have the conditional state being $|\psi\rangle_{B|y} \approx$

$$\frac{\sqrt{P_N[0]P_Q(|y|)}|\psi_0\rangle + \sqrt{P_N[1]P_Q(\sqrt{\pi} - |y|)}|\psi_1\rangle}{\sqrt{P_N[0]P_Q(|y|) + P_N[1]P_Q(\sqrt{\pi} - |y|)}}, \quad (72)$$

where

$$\begin{aligned} |\psi_0\rangle &= \int ds_B dt_B \xi(s_B, t_B) e^{i(-s_B \hat{p}_B + (t_B \mp \sqrt{\pi}) \hat{q}_B)} |\bar{+}\rangle_B \\ &= \int ds_B dt_B \xi(s_B, t_B \pm \sqrt{\pi}) e^{i(-s_B \hat{p}_B + t_B \hat{q}_B)} |\bar{+}\rangle_B, \end{aligned} \quad (73)$$

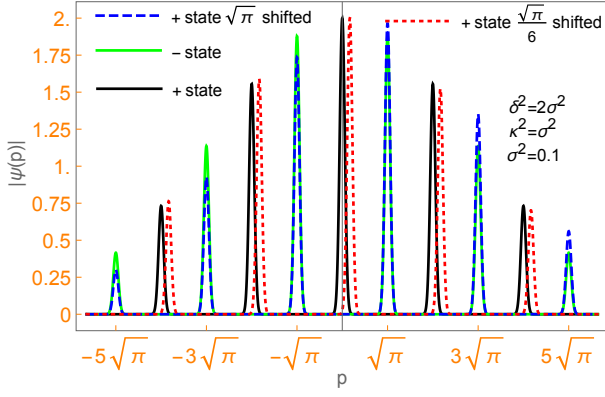


Figure 3. p -quadrature wavefunctions of $|\pm\rangle$ states of the form in (19-21) with $\delta^2/2 = \kappa^2 = \sigma^2 = 0.1$ (corresponds to 10 dB p -quadrature squeezing), and with and without mean shifts in the error wavefunction.

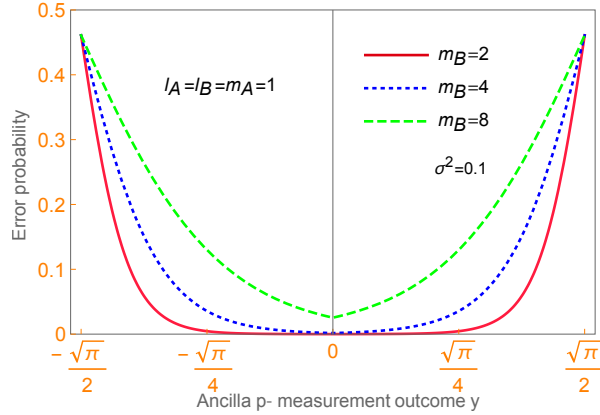


Figure 4. Mean displacement error probability as a function of the homodyne measurement outcome $|y| \leq \sqrt{\pi}/2$ for different values of m_B in (39), with $l_A = l_B = m_A = 1$ and $\sigma^2 = 0.1$.

and $|\psi_1\rangle$

$$\begin{aligned} &= \int ds_B dt_B \xi(s_B, t_B) e^{i(-s_B \hat{p}_B + (t_B + (1 \mp 1)\sqrt{\pi})\hat{q}_B)} |\mp\rangle_B \\ &= \int ds_B dt_B \xi(s_B, t_B - (1 \mp 1)\sqrt{\pi}) e^{i(-s_B \hat{p}_B + t_B \hat{q}_B)} |\mp\rangle_B, \end{aligned} \quad (74)$$

where the $|\psi_1(y)\rangle$ now is the state with support on the original underlying ideal GKP qubit state, whereas $|\psi_0(y)\rangle$ is the state with the orthogonal support. The $|\psi_1(y)\rangle$ term dominates in the superposition when $P_N[1]P_Q(\sqrt{\pi} - |y|)$ is larger than $P_N[0]P_Q(|y|)$.

More generally, consider the interval of measurement outcomes given by $n\sqrt{\pi} < |y| < (n+1)\sqrt{\pi}$. The probability $P_Y(y)$ of (48) for such an outcome $y \geq 0$ can be best approximated as

$$\begin{aligned} P_Y(y) &\approx P_N[n]P_Q(|y| - n\sqrt{\pi}) \\ &\quad + P_N[(n+1)]P_Q((n+1)\sqrt{\pi} - |y|). \end{aligned} \quad (75)$$

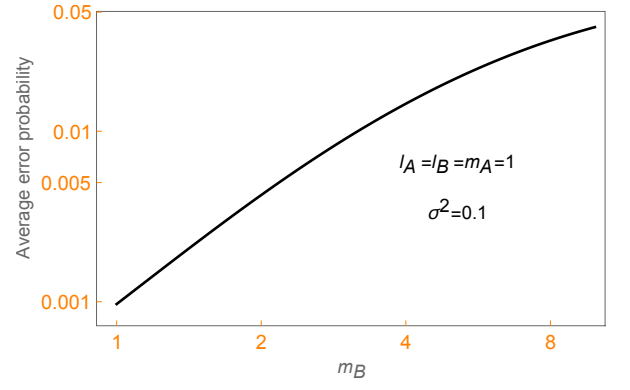


Figure 5. Average error probability when $|y| \leq \sqrt{\pi}/2$, as a function of m_B in (39), with $l_A = l_B = m_A = 1$ and $\sigma^2 = 0.1$.

When $m_A \ll m_B$, the error-corrected state is given by

$$|\psi\rangle_{B|y} \approx \frac{\sqrt{c_n}|\psi_n\rangle + \sqrt{c_{n+1}}|\psi_{n+1}\rangle}{\sqrt{c_n + c_{n+1}}}, \quad (76)$$

$$|\psi_n\rangle = \int ds_B dt_B \xi(s_B, t_B) e^{i(-s_B \hat{p}_B + (t_B + (n \mp 1)\sqrt{\pi})\hat{q}_B)} |+\rangle_B \quad (77)$$

$$|\psi_{n+1}\rangle = \int ds_B dt_B \xi(s_B, t_B) e^{i(-s_B \hat{p}_B + (t_B + (n+1 \mp 1)\sqrt{\pi})\hat{q}_B)} |+\rangle_B \quad (78)$$

$$c_n = P_N[n]P_Q(|y| - n\sqrt{\pi}) \quad (79)$$

$$c_{n+1} = P_N[(n+1)]P_Q((n+1)\sqrt{\pi} - |y|), \quad (80)$$

$$z = \begin{cases} n\sqrt{\pi}, & |y| - n\sqrt{\pi} < \sqrt{\pi}/2 \\ (n+1)\sqrt{\pi}, & \sqrt{\pi} > |y| - n\sqrt{\pi} > \sqrt{\pi}/2 \end{cases}. \quad (81)$$

The mean displacement error probability as a function of the measurement outcome y is thus given by

$$P_b(y) = \begin{cases} c_{n+1}/(c_n + c_{n+1}), & |y| - n\sqrt{\pi} < \sqrt{\pi}/2 \\ c_n/(c_n + c_{n+1}), & \sqrt{\pi} > |y| - n\sqrt{\pi} > \sqrt{\pi}/2 \end{cases}. \quad (82)$$

Figure 4 plots the error probability as a function of the homodyne outcome for $|y| \leq \sqrt{\pi}/2$ and different values of m_B in (39), with $l_A = l_B = m_A = 1$ and $\sigma^2 = 0.1$, while Fig. 5 plots the average value of the mean-displacement error probability for $|y| \leq \sqrt{\pi}/2$ (calculated as $\int dy P_Y(y)P_b(y)$) as a function of m_B .

Post-selection to minimize mean displacement error probability

Consider the case $|y| < \sqrt{\pi}$. The post-measurement state can be enhanced by suppressing the logically-flipped component in the coherent superposition in the conditional post-measurement state. This can be

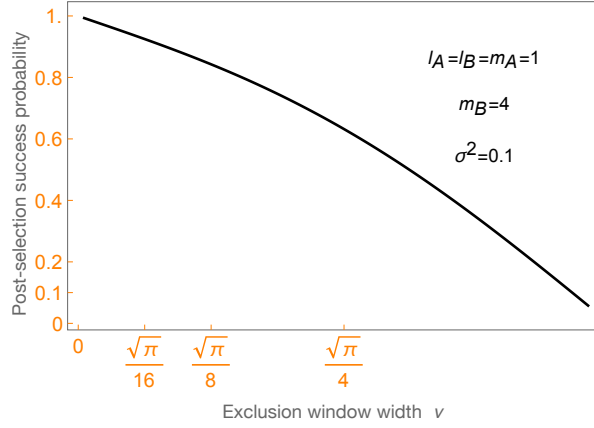


Figure 6. Post-selection success probability as a function of the exclusion window width ν in (83), for $l_A = l_B = m_A = 1$, $m_B = 4$ and $\sigma^2 = 0.1$ in (39).

| Feedback displacement | Residual Error |
|---|-------------------------------------|
| $g_T = \frac{1}{m_A} \frac{1}{2} H(\langle \Delta t_T^2 \rangle, m_A)$ | $\hat{Z}_T(g_T \sqrt{\pi})$ |
| $g_{N_i} = \frac{\langle \Delta s_{N_i} \Delta t_T \rangle}{\langle \Delta t_T^2 \rangle m_A} \frac{1}{2} H(\langle \Delta t_T^2 \rangle, m_A)$ | $\hat{X}_{N_i}(g_{N_i} \sqrt{\pi})$ |
| $g_{S_j} = \frac{\langle \Delta t_T \Delta t_{S_j} \rangle}{\langle \Delta t_T^2 \rangle m_A} \frac{1}{2} H(\langle \Delta t_T^2 \rangle, m_A)$ | $\hat{Z}_{S_j}(g_{S_j} \sqrt{\pi})$ |

Table I. Steane error correction: Gain factor for feedback displacement and the residual correlated mean displacement errors in neighboring (nearest N_i , next-to-nearest S_j) vertices of the target vertex. H here stands for the harmonic mean.

achieved by discarding outcomes in the interval $\sqrt{\pi}/2 - \nu \leq |y| \leq \sqrt{\pi}/2 + \nu$, $\sqrt{\pi}/2 > \nu > 0$ [34, 43] for the following reason. When $|y| \leq \sqrt{\pi}/2 - \nu$, the post-measurement state has $P_N[0]P_Q(|y|)/(P_N[1]P_Q(\sqrt{\pi} - |y|)) > 1$ that increases with increasing ν —i.e., the state $|\psi\rangle_{B|y} \approx |\psi_0(y)\rangle$ as ν increases. Likewise, when $\sqrt{\pi} > |y| \geq \sqrt{\pi}/2 + \nu$, the post-measurement state $|\psi\rangle_{B|y} \approx |\psi_1(y)\rangle$, increasingly so, as ν increases.

Of course, this enhancement comes with an associated post-selection success probability, a function of ν , given by

$$P_{\text{succ}}(\nu) = \int_{I_0(\nu)} dy P_Y(y) + \int_{I_1(\nu)} dy P_Y(y), \quad (83)$$

where $I_0(\nu) \equiv |y| \leq \sqrt{\pi}/2 - \nu$ and $I_1(\nu) \equiv \sqrt{\pi} > |y| \geq \sqrt{\pi}/2 + \nu$. Figure 6 plots the postselection success probability versus ν in (83) for $l_A = l_B = m_A = 1$, $m_B = 4$ and $\sigma^2 = 0.1$ in (39), while Fig. 7 plots the post-selection success probability versus average error probability tradeoff that ensues when varying ν .

B. Steane error correction on a vertex of a generic graph state

Now, consider a general finite-energy approximate GKP qubit graph state of the form in (23) and

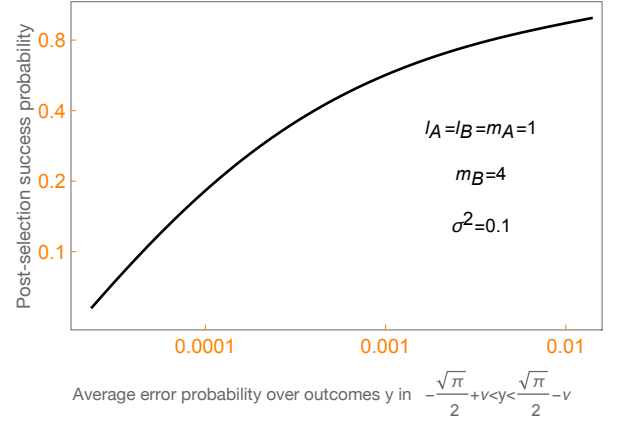


Figure 7. Post-selection success probability versus average error probability tradeoff by varying the post-selection exclusion window width ν in (83), for $l_A = l_B = m_A = 1$, $m_B = 4$ and $\sigma^2 = 0.1$ in (39).

| Q matrix | |
|---|---|
| Initial | Final |
| $\langle \Delta s_T^2 \rangle$ | $\langle \Delta s_T^2 \rangle + l_A$ |
| $\langle \Delta s_{N_i} \Delta s_{N_j} \rangle$ | $\langle \Delta s_{N_i} \Delta s_{N_j} \rangle - \frac{\langle \Delta s_{N_i} \Delta t_T \rangle \langle \Delta t_T \Delta s_{N_j} \rangle}{\langle \Delta t_T^2 \rangle m_A} \frac{1}{2} H(\langle \Delta t_T^2 \rangle, m_A)$ |
| P matrix | |
| Initial | Final |
| $\langle \Delta t_T^2 \rangle$ | $\frac{1}{2} H(\langle \Delta t_T^2 \rangle, m_A)$ |
| $\langle \Delta t_{S_i} \Delta t_{S_j} \rangle$ | $\langle \Delta t_{S_i} \Delta t_{S_j} \rangle - \frac{\langle \Delta t_T \Delta t_{S_i} \rangle \langle \Delta t_T \Delta t_{S_j} \rangle}{\langle \Delta t_T^2 \rangle m_A} \frac{1}{2} H(\langle \Delta t_T^2 \rangle, m_A)$ |
| $\langle \Delta t_T \Delta t_{S_j} \rangle$ | $\frac{\langle \Delta t_T \Delta t_{S_j} \rangle}{\langle \Delta t_T^2 \rangle} \frac{1}{2} H(\langle \Delta t_T^2 \rangle, m_A)$ |
| R matrix | |
| Initial | Final |
| $\langle \Delta s_{N_i} \Delta t_T \rangle$ | $\frac{\langle \Delta s_{N_i} \Delta t_T \rangle}{\langle \Delta t_T^2 \rangle} \frac{1}{2} H(\langle \Delta t_T^2 \rangle, m_A)$ |
| $\langle \Delta s_{N_i} \Delta t_{S_j} \rangle$ | $\langle \Delta s_{N_i} \Delta t_{S_j} \rangle - \frac{\langle \Delta s_{N_i} \Delta t_T \rangle \langle \Delta t_T \Delta t_{S_j} \rangle}{\langle \Delta t_T^2 \rangle m_A} \frac{1}{2} H(\langle \Delta t_T^2 \rangle, m_A)$ |

Table II. Steane error correction on a vertex of a graph state: Transformation of the elements of the error wavefunction covariance in (30) under Steane error correction, where T is the target, A refers to the ancilla, H refers to the harmonic mean, and N and S refer to the nearest and second nearest neighbors to the target T , respectively. The matrix elements not mentioned above remain unchanged.

p -quadrature Steane error correction of an arbitrary vertex T of the graph using ancilla A . When the outcome of the measurement on the ancilla is y such that $|y| < \sqrt{\pi}/2$ and when $m_A \ll m_T$, the Graph state transforms as $|\widetilde{\Psi}_G(y)\rangle$

$$\approx \frac{\sqrt{P_N[0]P_Q(|y|)}|\widetilde{\Psi}_0\rangle + \sqrt{P_N[1]P_Q(\sqrt{\pi} - |y|)}|\widetilde{\Psi}_1\rangle}{\sqrt{P_N[0]P_Q(|y|) + P_N[1]P_Q(\sqrt{\pi} - |y|)}}, \quad (84)$$

where

$$|\widetilde{\Psi}_0\rangle = \int d\vec{s} d\vec{t} \xi_G(\vec{s}, \vec{t}) e^{i(-\vec{s} \cdot \vec{p} + \vec{t} \cdot \vec{q})} |\overline{\Psi}_G\rangle, \quad (85)$$

$$\begin{aligned} |\widetilde{\Psi}_1\rangle &= \int d\vec{s} d\vec{t} \xi_G(\vec{s}, \vec{t}) e^{i(-(\vec{s} + \vec{s}') \cdot \vec{p} + (\vec{t} + \vec{t}') \cdot \vec{q})} |\overline{\Psi}_G\rangle \\ &= \int d\vec{s} d\vec{t} \xi_G(\vec{s} - \vec{s}', \vec{t} - \vec{t}') e^{i(-\vec{s} \cdot \vec{p} + \vec{t} \cdot \vec{q})} |\overline{\Psi}_G\rangle \end{aligned} \quad (86)$$

(up to phase factors $\exp(-is_T l_A / (l_A + l_T) n \sqrt{\pi})$, $n \in \{0, 1\}$) and $P_N[n]$ and $P_Q(p)$ are Gaussian distributions of integer-valued and real-valued random variables N and Q given in (49) and (50), respectively, with $\{l_B, m_B\}$ replaced by $\{l_T, m_T\}$. The vectors \vec{s}', \vec{t}' in $|\widetilde{\Psi}_1\rangle$ are residual displacement errors on the qubits, given by $\vec{s}' = \{g_{N_i} \sqrt{\pi}\}$, $\vec{t}' = \{g_T \sqrt{\pi}, g_{S_j} \sqrt{\pi}\}$, whose entries are 0 except at T (target), N_i (nearest neighboring) and S_j (next-to-nearest neighboring) vertices, with the latter entry values as given in Table I. The g values of Table I are in fact the gain factors used in applying the feedback displacement on the graph state qubits as part of the Steane error correction procedure.

Thus, under Steane error correction, a finite-energy GKP qubit graph state transforms into a conditional output, which is a superposition of finite-energy GKP qubit graph states whose error wavefunctions $\xi_G(\vec{x})$ are given by square roots of Gaussian distribution functions with identical covariance matrices of the form in (30), but with different mean displacement vectors. The state $|\widetilde{\Psi}_1\rangle$ represents the displacement error term in the state $|\Psi_G(y)\rangle$ of (84) and the probability associated with this error is given by (79)-(82), which is a function of the homodyne measurement outcome y . Note that post-selection can be used to reduce the error probability similarly as discussed for the single qubit case earlier. The transformation rules for the elements of the covariance matrix of $\xi_G(\vec{x})$ in terms of the elements of the pre-Steane error correction covariance matrix are given in Table II.

V. FUSION OPERATIONS

In linear optical quantum computing with single-photon-based qubits, graph states that are universal for measurement-based quantum computing can be created by fusing small graph states using rotated Bell state measurements, or fusions [48]. In this section, we explore the CV analogue of such fusions that can be similarly used to grow GKP qubit graph states. One important thing to note here is that whereas linear optical single-photon-based fusions fail when particular photon detection patterns are not observed at the detectors [48], the fusion for GKP qubits always succeeds as long as no post-selection is performed on the measurement outcomes. Below, we discuss three CV circuits for fusions, denoted as Types A, B, and C. Types A and B are based on the CV C_X gate (shown in Figs. 8 and 9), which require inline squeezing along with beam splitters, phase shifters and homodyne

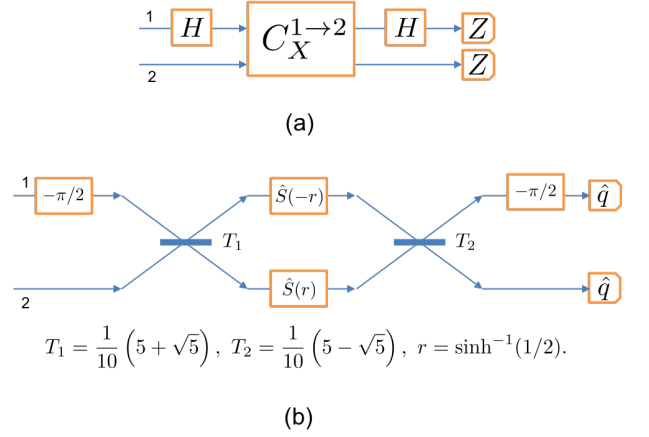


Figure 8. Type A fusion: (a) circuit diagram and (b) its optical implementation. In (a), H is the Hadamard gate, C_X is the controlled-NOT gate and Z denotes standard-basis measurement. In (b) $-\pi/2$ is a phase rotation, T_1, T_2 are beam-splitter transmissivities, \hat{S} denotes a single-mode squeezer and \hat{q} denotes q -quadrature measurement.

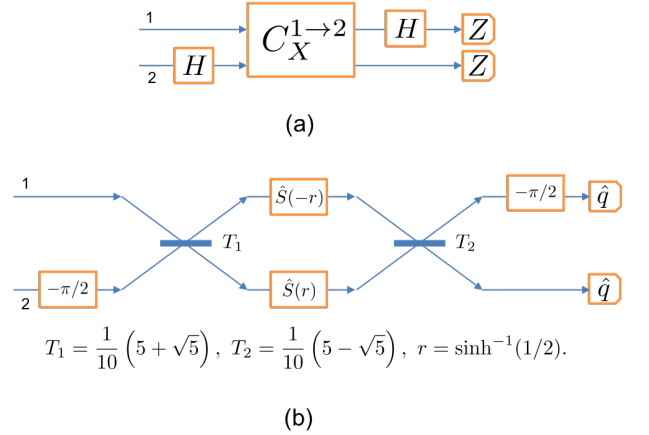


Figure 9. Type B fusion.

detection. On the other hand, Type C is based on the so-called dual homodyne CV measurement, which does not require inline squeezing (shown in Fig. 10). The dual homodyne measurement is used, e.g., in CV Gaussian entanglement swapping. When acted on ideal infinite-energy GKP qubits, all the three CV fusions perform rotated Bell-state measurements given by the set of pro-

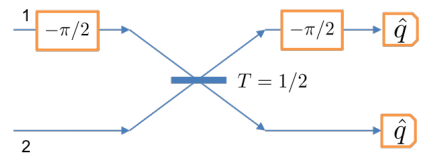


Figure 10. Type C fusion.

| Q matrix | |
|---|--|
| Initial | Final |
| $\langle \Delta s_{N_{k,i}} \Delta s_{N_{k,j}} \rangle$ | $\langle \Delta s_{N_{k,i}} \Delta s_{N_{k,j}} \rangle - \frac{\langle \Delta s_{N_{k,i}} \Delta t_k \rangle \langle \Delta s_{N_{k,j}} \Delta t_k \rangle}{\langle \Delta t_k^2 \rangle + \langle \Delta s_{k'}^2 \rangle}$ |
| P matrix | |
| Initial | Final |
| $\langle \Delta t_{N_{k,i}} \Delta t_{N_{k,j}} \rangle$ | $\langle \Delta t_{N_{k,i}} \Delta t_{N_{k,j}} \rangle - \frac{\langle \Delta s_{N_{k,i}} \Delta t_k \rangle \langle \Delta s_{N_{k,j}} \Delta t_k \rangle}{\langle \Delta s_k^2 \rangle + \langle \Delta t_{k'}^2 \rangle}$ |
| $\langle \Delta t_{S_{k,i}} \Delta t_{S_{k,j}} \rangle$ | $\langle \Delta t_{S_{k,i}} \Delta t_{S_{k,j}} \rangle - \frac{\langle \Delta s_{N_{k,i}} \Delta t_k \rangle \langle \Delta s_{N_{k,j}} \Delta t_k \rangle}{\langle \Delta t_k^2 \rangle + \langle \Delta s_{k'}^2 \rangle}$ |
| R matrix | |
| Initial | Final |
| $\langle \Delta s_{N_{k,i}} \Delta t_{S_{k,j}} \rangle$ | $\langle \Delta s_{N_{k,i}} \Delta t_{S_{k,j}} \rangle + \frac{\langle \Delta s_{N_{k,i}} \Delta t_k \rangle \langle \Delta s_{N_{k,j}} \Delta t_k \rangle}{\langle \Delta t_k^2 \rangle + \langle \Delta s_{k'}^2 \rangle}$ |

Table III. Transformation of the error wavefunction covariance matrices under all 3 types of fusion. N_k and S_k refer to the set of nearest and second nearest neighbors to the fused modes $k \in \{C, T\}$, respectively, where C, T stand for the control and target modes. The matrix elements not mentioned above remain unchanged.

vectors $\{|\psi_{i,j}\rangle\langle\psi_{i,j}|, (i,j) \in \{0,1\}^2\}$, where

$$\begin{aligned}
|\psi_{00}\rangle &= |0, +\rangle + |1, -\rangle = |+, 0\rangle + |-, 1\rangle, \\
|\psi_{10}\rangle &= |0, +\rangle - |1, -\rangle = |+, 0\rangle - |-, 1\rangle, \\
|\psi_{01}\rangle &= |0, -\rangle + |1, +\rangle = |-, 0\rangle + |+, 1\rangle, \\
|\psi_{11}\rangle &= |0, -\rangle - |1, +\rangle = |-, 0\rangle - |+, 1\rangle.
\end{aligned} \quad (87)$$

However, when acted on finite-energy approximate GKP qubits, which form the subject of this present work, the projections applied by these circuits are no longer equivalent. They result in different conditional output states. The fusions can be followed by suitable feedback displacements on the vertices of the fused graph, which can be chosen in such a way as to remove the dependence of the resulting graph state on the measurement outcomes. It turns out that feedback displacements are required to be performed on only up to the second nearest neighbors of the vertices corresponding to the control qubit C and the target qubit T in the input sub-graph states.

The underlying graph structure of the resulting graph state following fusion is governed by the action of the fusion on the underlying ideal GKP qubit graph state. In this regard, as a result of their identical actions on ideal GKP qubits, all the three types of fusions, similar to the case of single-photon-based qubits, connect all neighbours of qubit C and qubit T with each other [49].

Consider 2 subgraph states $|\widetilde{\Psi}_{G_j}\rangle =$

$$\int d\vec{x} \, \eta_{G_j}(\vec{\mu}, V, \vec{x}) \prod_{i=1}^n e^{\frac{i x_i x_{n+i}}{2}} \hat{X}(x_i) \hat{Z}(x_{n+i}) |\widetilde{\Psi}_{G_j}\rangle, \quad j \in \{1, 2\} \quad (88)$$

of the form in (23), as described in Section III and identify two vertices C and T , one from each of the two sub-graphs. When a fusion operation is applied from C to T , and the measurement outcomes are $|y_C\rangle, |y_T\rangle \leq \sqrt{\pi}/2$, the post-fusion (followed by feedback displacements on

| Mean vector elements | |
|-----------------------------|--|
| Initial | Final |
| $\mu'_{q_{C_i}}{}^{(10)}$ | $\mu_{q_{C_i}} + \begin{cases} \frac{\langle \Delta s_{C_i} \Delta t_C \rangle}{\langle \Delta t_C^2 \rangle} \times \sqrt{\pi}, & \text{if } C_i \in N_C \\ 0, & \text{otherwise.} \end{cases}$ |
| Mean vector elements Type B | |
| Initial | Final |
| $\mu'_{p_{T_i}}{}^{(10)}$ | $\mu_{p_{T_i}} + \begin{cases} -\frac{\langle \Delta t_{T_i} \Delta s_C \rangle}{\langle \Delta s_C^2 \rangle} \times \sqrt{\pi}, & \text{if } T_i \in N_C \\ -\frac{\langle \Delta t_{T_i} \Delta s_T \rangle}{\langle \Delta s_T^2 \rangle} \times \sqrt{\pi}, & \text{if } T_i \in N_T \\ 0, & \text{otherwise.} \end{cases}$ |
| Mean vector elements Type C | |
| Initial | Final |
| $\mu'_{q_{C_i}}{}^{(10)}$ | $\mu_{q_{C_i}} + \begin{cases} -\frac{\langle \Delta s_{C_i} \Delta t_C \rangle}{\langle \Delta t_C^2 \rangle + \langle \Delta s_T^2 \rangle} \times \sqrt{2\pi}, & \text{if } C_i \in N_C \\ 0, & \text{otherwise.} \end{cases}$ |
| $\mu'_{p_{C_i}}{}^{(10)}$ | $\mu_{p_{C_i}} + \begin{cases} -\frac{\langle \Delta t_C^2 \rangle + \langle \Delta s_T^2 \rangle}{\langle \Delta s_{C_i} \Delta t_C \rangle} \times \sqrt{2\pi}, & \text{if } C_i \in N_C \\ +\frac{\langle \Delta s_{C_i} \Delta t_C \rangle}{\langle \Delta t_C^2 \rangle + \langle \Delta s_T^2 \rangle} \times \sqrt{2\pi}, & \text{if } C_i \in S_C \\ 0, & \text{otherwise.} \end{cases}$ |

Table IV. Transformation of the error wavefunction mean vector elements under fusion Types A, B and C. N_k and S_k refer to the set of nearest and second nearest neighbors to the fused modes $k \in \{C, T\}$, respectively, where C, T stand for the control and target modes. here if k is C , then k' is T and vice versa. The matrix elements not mentioned above remain unchanged.

up to second-nearest neighboring vertices of C and T), the state is given by $|\widetilde{\Psi}'_G\rangle_{|y_C, y_T} \propto \approx$

$$\begin{aligned}
& \sqrt{P_{N_C}[0] P_{Q_C}(|y_C\rangle) P_{N_T}[0] P_{Q_T}(|y_T\rangle)} |\widetilde{\psi}'^{(00)}_G\rangle \\
& + \sqrt{P_{N_C}[0] P_{Q_C}(|y_C\rangle) P_{N_T}[1] P_{Q_T}(\sqrt{\pi} - |y_T\rangle)} |\widetilde{\psi}'^{(01)}_G\rangle \\
& + \sqrt{P_{N_C}[1] P_{Q_C}(\sqrt{\pi} - |y_C\rangle) P_{N_T}[0] P_{Q_T}(|y_T\rangle)} |\widetilde{\psi}'^{(10)}_G\rangle \\
& + \sqrt{P_{N_C}[1] P_{Q_C}(\sqrt{\pi} - |y_C\rangle) P_{N_T}[1] P_{Q_T}(\sqrt{\pi} - |y_T\rangle)} \\
& \times |\widetilde{\psi}'^{(11)}_G\rangle
\end{aligned} \quad (89)$$

where $|\widetilde{\psi}'^{(uv)}_G\rangle \equiv G(\mathcal{V}', \mathcal{E}', \vec{\mu}'^{(uv)}, V')$, $u, v \in \{0, 1\}$, $|\mathcal{V}'| = n - 2$ and the topology of the fused graph \mathcal{E}' can be found in Ref. [49]. The transformation rules for the error wave function covariance matrix and mean displacement elements of these conditional graph states $|\widetilde{\psi}'^{(uv)}_G\rangle$, namely $V', \vec{\mu}'^{(uv)}$, under the fusion operations A, B and C in terms of the pre-fusion covariance matrix elements and mean displacement vector are tabulated in Tables III and IV, respectively. All terms in the superposition in (89) except the one corresponding to $u = v = 0$ are error terms, whose probabilities are given by their coefficients in the superposition upto suitable normalization. The error probabilities are functions of y_C, y_T , and similar to Steane error correction, could be reduced using post selection.

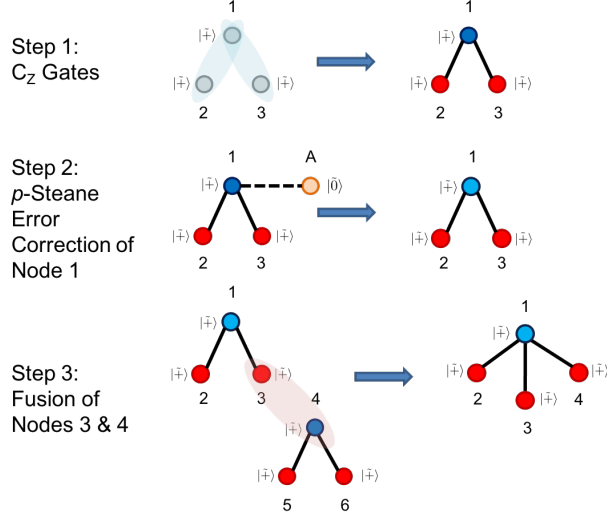


Figure 11. Generation of a 4-qubit tree graph state from finite-energy approximate GKP qubits using C_Z gate, Steane error correction and Fusion operations, as per the protocol presented Ref. [43]

| Type | Covariance Matrix |
|-------|---|
| A,B,C | $\sigma^2 \begin{pmatrix} \frac{5}{3} & 0 & 0 & 0 & 0 & -\frac{2}{3} & \frac{1}{3} & \frac{1}{3} \\ 0 & \frac{11}{15} & \frac{1}{15} & \frac{1}{15} & -\frac{4}{15} & 0 & 0 & 0 \\ 0 & \frac{1}{15} & \frac{11}{15} & -\frac{4}{15} & \frac{1}{15} & 0 & 0 & 0 \\ 0 & \frac{1}{15} & -\frac{4}{15} & \frac{11}{15} & \frac{1}{15} & 0 & 0 & 0 \\ 0 & -\frac{4}{15} & \frac{1}{15} & \frac{1}{15} & \frac{11}{15} & 0 & 0 & 0 \\ -\frac{2}{3} & 0 & 0 & 0 & 0 & \frac{5}{3} & -\frac{1}{3} & -\frac{1}{3} \\ \frac{1}{3} & 0 & 0 & 0 & 0 & -\frac{1}{3} & \frac{5}{3} & \frac{1}{3} \\ \frac{1}{3} & 0 & 0 & 0 & 0 & -\frac{1}{3} & \frac{1}{3} & \frac{5}{3} \end{pmatrix}$ |

Table V. Covariance Matrix of the error wavefunctions at the output of the protocol described in Fig. 11. It is the same independent of the type of fusion applied. The quadratures are ordered as $(q_1, \dots, q_4, p_1, \dots, p_4)$.

| Type | Mean Displacement Vectors |
|------|--|
| A | $\left\{ -\frac{\sqrt{\pi}}{3}u, \frac{\sqrt{\pi}}{15}(-4w+v), \frac{\sqrt{\pi}}{15}(w-4v), \frac{\sqrt{\pi}}{15}(w-4v), \right.$ $\left. \frac{\sqrt{\pi}}{15}(11w+v), \frac{\sqrt{\pi}u}{3}, \frac{\sqrt{\pi}u}{3}, \frac{\sqrt{\pi}u}{3} \right\}$ |
| B | $\left\{ \frac{\sqrt{\pi}}{3}v, \frac{\sqrt{\pi}}{15}(-4w+u), \frac{\sqrt{\pi}}{15}(w-4u), \frac{\sqrt{\pi}}{15}(w-4u), \right.$ $\left. \frac{\sqrt{\pi}}{15}(11w+u), -\frac{\sqrt{\pi}}{3}v, -\frac{\sqrt{\pi}}{3}v, -\frac{\sqrt{\pi}}{3}v \right\}$ |
| C | $\left\{ \frac{\sqrt{2\pi}}{3}u, \frac{\sqrt{\pi}}{15}(-4w+\sqrt{2}v), -\frac{\sqrt{\pi}}{15}(w-4\sqrt{2}v), \right.$ $\left. -\frac{\sqrt{\pi}}{15}(w-4\sqrt{2}v), \frac{\sqrt{\pi}}{15}(11w+\sqrt{2}v), \right.$ $\left. -\frac{\sqrt{2\pi}}{3}u, \frac{\sqrt{2\pi}}{3}u, \frac{\sqrt{2\pi}}{3}u \right\}$ |

Table VI. Error wavefunction mean displacement vectors of the finite-energy GKP-qubit graph states that are in coherent superposition at the output of the protocol described in Fig. 11, for the different choice of fusion operations between types A, B and C. The quadratures are ordered as $(q_1, \dots, q_4, p_1, \dots, p_4)$. The different tuples of indices $u, v, w \in \{0, 1\}$ correspond to the 8 terms that are in superposition.

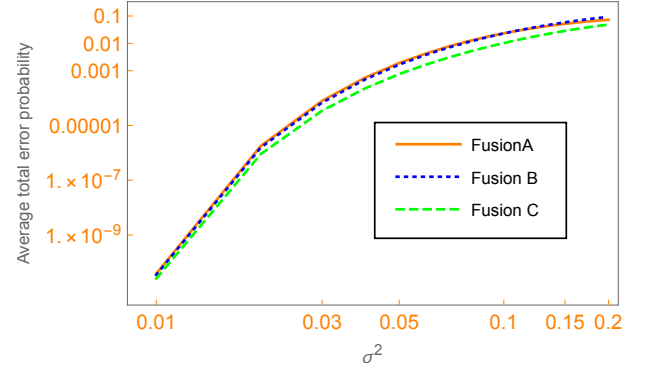


Figure 12. Average total error probability associated with the generation of the 4-qubit tree graph state from finite-energy approximate GKP qubits using the protocol presented Ref. [43] with the three different fusions discussed in Sec V, as a function of σ^2 , where the initial finite-energy approximate GKP qubits have teeth and envelope variances given by $\sigma^2/2, 1/2\sigma^2$, respectively.

VI. DISCUSSION

The tools discussed in Sections IV and V can be used to generate fault-tolerant graph states starting from finite-energy approximate GKP qubit $|+\rangle$ states. Ref. [43] provided a protocol to generate graph states starting from mixed state GKP qubits that are defined as incoherent Gaussian mixtures of randomly displaced ideal GKP qubit states. Such states can be obtained from the pure finite-energy GKP qubit states considered in this work by a Gaussian displacement twirling operation, and thus by the data-processing inequality, are more noisy. An approach similar to the one in Ref. [43] can be adopted to generate universal GKP graph states from the pure, finite energy approximate GKP qubit states considered here using fusions and Steane error correction in a ballistic fashion similar to discrete-variable linear optical schemes [42].

As a demonstration of our analysis, we look at the generation of a small 4-qubit tree cluster made of finite-energy approximate GKP qubits, tracing the first few steps of the protocol followed in Ref. [43]. The protocol is described step by step in Fig. 11. While the analysis in Ref. [43] tracked the individual quadrature noise variances of mixed state GKP qubits, our analysis with truly finite energy GKP qubits tracks the full covariance matrix of the Gaussian error wavefunction of the graph state along with the mean displacement vector. This work thus provides a more accurate analysis of the errors that are introduced during the graph creation from approximate GKP qubit pure states due to (a) the finite-energy approximation, and (b) homodyne measurements that are part of the graph state generation protocol. Since the 4-qubit tree cluster generation as per the protocol involves 1 steane error correction and 1 fusion operation, there are 3 homodyne measurements. This results in a total

of 8 terms in superposition at the output, which correspond to finite-energy GKP qubit graph states whose error wavefunctions $\xi_G(\vec{x})$ are given by square roots of Gaussian distribution functions with identical covariance matrices of the form in (30) given in Table V, but with different mean displacement vectors, as tabulated in Table VI indexed by $u, v, w \in \{0, 1\}$. The total error probability, i.e., the norm of the weights associated with all but the term corresponding to $u = v = w = 0$ in the superposition, averaged over the outcomes homodyne measurement outcomes in the Steane error correction and the fusion, are plotted for the 3 types of fusion in Fig. 12 as function of initial GKP-qubit squeezing variance σ^2 . We observe that the error probabilities with all three Fusions converge in the ideal limit of small variance, while at larger variances Fusion C results in marginally lesser average error compared to Fusions A and B. The error probabilities can be further reduced by considering post-selected homodyne measurements as part of both the Steane error correction and fusion, as discussed earlier in Sec. IV A.

In summary, we presented an exact description of graph states composed of truly finite-energy, approximate GKP qubit pure states in terms of Gaussian error wavefunctions. We presented rules for the transformation of the error wavefunction's covariance matrix and mean vector under Steane error correction and graph fusion operations that are used to generate high-fidelity large graph states. The output of these procedures in the coherent error wavefunction description are coherent superpositions of 2^n number of approximate GKP qubit graph states (n being the number of homodyne measurement involved) whose error wavefunctions have identical covariance matrices, but different mean displacement vectors, all of which except one correspond to mean displacement errors in phase space. The error probabilities are functions of the homodyne measurement output statistics and can be reduced using post-selection generation of graph states at the expense of finite success probability of graph state generation. Whereas studies hitherto on GKP qubit graph states have dealt with incoherent, mixed state descriptions of GKP qubits, our work presents an accurate model for the noise and displacement errors present in graph states composed of finite-energy GKP qubits. Our work thus could potentially be useful in generating and characterizing the error correction properties of large graph states for measurement-based quantum information processing with applications in quantum computing and all-optical quantum repeaters.

ACKNOWLEDGMENTS

K.P.S. and P.D. acknowledge funding support from a Department of Energy (DoE) project on continuous variable quantum repeaters, funded under a subcontract from ORNL, subcontract number 4000178321. A.P., L.J. and S.G. acknowledge support of the Na-

tional Science Foundation (NSF) ERC, Center for Quantum Networks, award number 1941583. L.J. acknowledges support from the ARO (W911NF-18-1-0020, W911NF-18-1-0212), ARO MURI (W911NF-16-1-0349), AFOSR MURI (FA9550-19-1-0399), NSF (EFMA-1640959, OMA-1936118, EEC-1941583), NTT Research, and the Packard Foundation (2013-39273). S.G., K.P.S. and A.P. gratefully acknowledge several useful discussions with Rafael Alexander, and various researchers at Xanadu Quantum Technologies, esp., Ish Dhand, Krishnakumar Sabapathy, Guillaume Dauphinais, and Ilan Tzitrin. K.P.S. gratefully acknowledges several useful discussions with Filip Rozpedek.

CONFLICT OF INTEREST

S.G. serves as a scientific advisor for Xanadu Quantum Technologies, a company pursuing fault-tolerant quantum computing with photonic GKP qubits. S.G. owns stock options in the company and has received financial compensation for his technical advisory services. The other authors declare no conflicts of interest.

Appendix A: Equivalence between error wavefunction and quadrature-basis descriptions of GKP qubit states.

Here we show the equivalence between the error wavefunction description and quadrature-basis description of a GKP qubit state. Consider as an example, the $|\tilde{+}\rangle$ state. Without loss of generality, assuming zero mean displacements, we have

$$|\tilde{+}\rangle = \int dudv \frac{1}{\sqrt{\pi\kappa\delta}} \exp\left(-\frac{1}{2}(u^2/\delta^2 + v^2/\kappa^2)\right) \exp(i(-u\hat{p} + v\hat{q}))|\bar{+}\rangle, \quad (\text{A1})$$

$$= \int dudv \frac{1}{\sqrt{\pi\kappa\delta}} \exp\left(-\frac{1}{2}(u^2/\delta^2 + v^2/\kappa^2)\right) \exp(iuv/2)\hat{X}(u)\hat{Z}(v)|\bar{+}\rangle, \quad (\text{A2})$$

which follows from (2). Proceeding further, we have

$$|\tilde{+}\rangle = \sum_{n=-\infty}^{\infty} \frac{1}{\sqrt{\pi\kappa\delta}} \int du e^{\frac{iuv}{2}} e^{-\frac{u^2}{2\delta^2}} e^{-iu(2n\sqrt{\pi}+v)} \times \int dv e^{-\frac{v^2}{2\kappa^2}} |p = 2n\sqrt{\pi} + v\rangle, \quad (\text{A3})$$

where $|\bar{+}\rangle$ has been expanded in the basis of p -eigenstates, and the action of the \hat{X} operator on these states results in the factor $e^{-iu(2n\sqrt{\pi}+v)}$. The above state

can be reexpressed as

$$|\tilde{+}\rangle = \sum_{n=-\infty}^{\infty} \frac{\sqrt{2\pi\delta^2}}{\sqrt{\pi\kappa\delta}} \int du \frac{e^{-\frac{u^2}{2\delta^2}}}{\sqrt{2\pi\delta^2}} e^{-iu(2n\sqrt{\pi}-v/2)} \int dv e^{-\frac{v^2}{2\kappa^2}} \hat{Z}(2n\sqrt{\pi}+v)|p=0\rangle \quad (\text{A4})$$

$$= \sqrt{\frac{2\delta}{\kappa}} \sum_n \int dv e^{-\frac{(2n\sqrt{\pi}+v/2)^2\delta^2}{2}} e^{-\frac{v^2}{2\kappa^2}} \hat{Z}(2n\sqrt{\pi}+v)|p=0\rangle, \quad (\text{A5})$$

which follows from evaluating the Fourier intergral in variable u . The above equation can be re-expressed with completion of squares in variable v as

$$|\tilde{+}\rangle = \sqrt{\frac{2\delta}{\kappa}} \sum_n e^{-\frac{8\pi\delta^2}{4+\kappa^2\delta^2}n^2} \int dv e^{-\frac{\left(v+\frac{4\sqrt{\pi}\delta^2\kappa^2n}{4+\delta^2\kappa^2}\right)^2}{\frac{8\kappa^2}{4+\delta^2\kappa^2}}} \hat{Z}(2n\sqrt{\pi}+v)|p=0\rangle \quad (\text{A6})$$

$$= \sqrt{2\pi} \sum_n \frac{e^{-\frac{(2\sqrt{\pi}n)^2}{2\left(\frac{4+\delta^2\kappa^2}{4\delta^2}\right)}}}{\left(\pi\left(\frac{4+\delta^2\kappa^2}{4\delta^2}\right)\right)^{1/4}} \int dv \frac{e^{-\frac{\left(v+\frac{4\sqrt{\pi}\delta^2\kappa^2n}{4+\delta^2\kappa^2}\right)^2}{\frac{8\kappa^2}{4+\delta^2\kappa^2}}}}{\left(\pi\left(\frac{4\kappa^2}{4+\delta^2\kappa^2}\right)\right)^{1/4}} \hat{Z}(2n\sqrt{\pi}+v)|p=0\rangle. \quad (\text{A7})$$

In the limit $\kappa^2\delta^2 \rightarrow 0$, we get

$$|\tilde{+}\rangle = \sqrt{2\pi} \sum_n \frac{e^{-\frac{\delta^2(2\sqrt{\pi}n)^2}{2}}}{(\pi/\delta^2)^{1/4}} \int dv \frac{e^{-\frac{v^2}{2\kappa^2}}}{(\pi\kappa^2)^{1/4}} \hat{Z}(2n\sqrt{\pi}+v)|p=0\rangle, \quad (\text{A8})$$

thus showing the equivalence between the error wavefunction and quadrature wavefunction descriptions.

Appendix B: Steane Error Correction Details

When mode A is measured over its p -quadrature, we get an outcome $y \in \mathbb{R}$ with probability $P_Y(y)$ and a conditional state $|\phi\rangle_{B|y}$ on mode B , that can be deduced

from the conditional unnormalized state given by

$$p\langle y|_A \cdot |\psi\rangle_{AB} = \sqrt{P_Y(y)} |\phi\rangle_{B|y} = \int ds_A ds_B \chi_{AB}(s_A, s_B) \int dt_A dt_B \mathcal{P}(t_A) \mathcal{Q}(t_B|t_A) p\langle y|_A \cdot e^{i(-s_A \hat{p}_A + t_A \hat{q}_A)} |\bar{0}\rangle_A e^{i(-s_B \hat{p}_B + t_B \hat{q}_B)} |\bar{+}\rangle_B \quad (\text{B1})$$

$$= \sum_n \int ds_A ds_B \chi_{AB}(s_A, s_B) \int dt_A dt_B \mathcal{P}(t_A) \mathcal{Q}(t_B|t_A) p\langle y|_A \cdot e^{\frac{is_A t_A}{2}} \hat{X}_A(s_A) \hat{Z}_A(t_A) |n\sqrt{\pi}\rangle_{p_A} e^{i(-s_B \hat{p}_B + t_B \hat{q}_B)} |\bar{+}\rangle_B \quad (\text{B2})$$

$$= \sum_n \int ds_A ds_B \chi_{AB}(s_A, s_B) \int dt_A dt_B \mathcal{P}(t_A) \mathcal{Q}(t_B|t_A) e^{\frac{is_A t_A}{2}} p\langle y|_A \cdot \hat{X}_A(s_A) |n\sqrt{\pi} + t_A\rangle_{p_A} e^{i(-s_B \hat{p}_B + t_B \hat{q}_B)} |\bar{+}\rangle_B \quad (\text{B3})$$

$$= \sum_n \int ds_A ds_B \chi_{AB}(s_A, s_B) \int dt_A dt_B \mathcal{P}(t_A) \mathcal{Q}(t_B|t_A) e^{-is_A(n\sqrt{\pi} + \frac{t_A}{2})} \delta(y - (n\sqrt{\pi} + t_A)) e^{i(-s_B \hat{p}_B + t_B \hat{q}_B)} |\bar{+}\rangle_B \quad (\text{B4})$$

$$= \sum_n \int ds_A ds_B \chi_{AB}(s_A, s_B) \int dt_A dt_B \mathcal{P}(t_A) \mathcal{Q}(t_B|t_A) e^{-is_A(n\sqrt{\pi} + \frac{t_A}{2})} \delta(t_A - (y - n\sqrt{\pi})) e^{i(-s_B \hat{p}_B + t_B \hat{q}_B)} |\bar{+}\rangle_B \quad (\text{B5})$$

$$= \sum_n \int ds_A ds_B dt_B \chi_{AB}(s_A, s_B) \mathcal{P}(t_A = y - n\sqrt{\pi}) \mathcal{Q}(t_B|t_A = y - n\sqrt{\pi}) e^{\frac{-is_A(y+n\sqrt{\pi})}{2}} e^{i(-s_B \hat{p}_B + t_B \hat{q}_B)} |\bar{+}\rangle_B. \quad (\text{B6})$$

Using the distributions for $\chi, \mathcal{P}, \mathcal{Q}$ from (43), we have

$$= \sum_n \frac{e^{-\frac{(y-n\sqrt{\pi})^2}{2(m_A+m_B)\sigma^2}}}{(\pi(m_A+m_B)\sigma^2)^{1/4}} \int ds_B dt_B \int ds_A \chi_{AB}(s_A, s_B) e^{\frac{-is_A(y+n\sqrt{\pi})}{2}} \frac{e^{-\frac{\left(t_B + \frac{m_B}{m_A+m_B}(y-n\sqrt{\pi})\right)^2}{2\frac{m_A m_B}{m_A+m_B}\sigma^2}}}{\left(\pi\frac{m_A m_B}{m_A+m_B}\sigma^2\right)^{1/4}} e^{i(-s_B \hat{p}_B + t_B \hat{q}_B)} |\bar{+}\rangle_B \quad (\text{B7})$$

$$= 2\sqrt{\pi} \sum_n \frac{e^{-\frac{(y-n\sqrt{\pi})^2}{2(m_A+m_B)\sigma^2}}}{(\pi(m_A+m_B)\sigma^2)^{1/4}} \frac{e^{-\frac{(y+n\sqrt{\pi})^2}{8\frac{(l_A+l_B)}{l_A l_B}\sigma^2}}}{(4\pi\frac{(l_A+l_B)}{l_A l_B}\sigma^2)^{1/4}} \times \left(\int ds_B dt_B \frac{e^{-\frac{s_B^2}{2(l_A+l_B)\sigma^2}}}{(\pi(l_A+l_B)\sigma^2)^{1/4}} \frac{e^{-\frac{\left(t_B + \frac{m_B}{m_A+m_B}(y-n\sqrt{\pi})\right)^2}{2\frac{m_A m_B}{m_A+m_B}\sigma^2}}}{\left(\pi\frac{m_A m_B}{m_A+m_B}\sigma^2\right)^{1/4}} e^{-i\frac{l_A}{2(l_A+l_B)}(y+n\sqrt{\pi})s_B} e^{i(-s_B \hat{p}_B + t_B \hat{q}_B)} |\bar{+}\rangle_B \right) \quad (\text{B8})$$

Appendix C: Shifted error wavefunction

Consider the example of an approximate GKP qubit state whose underlying GKP qubit state is the $|\bar{+}\rangle$, and error wavefunction has non-zero mean displacements given by u' and v' , i.e.,

$$|\tilde{\psi}\rangle = \int dudv \frac{e^{-\frac{(u-u')^2}{2\delta^2} - \frac{(v-v')^2}{2\kappa^2}}}{\sqrt{\pi\kappa\delta}} e^{i(-u\hat{p}+v\hat{q})} |\bar{+}\rangle, \quad (\text{C1})$$

$$= \int dudv \frac{e^{-\frac{(u-u')^2}{2\delta^2} - \frac{(v-v')^2}{2\kappa^2}}}{\sqrt{\pi\kappa\delta}} e^{\frac{iuv}{2}} \hat{X}(u) \hat{Z}(v) |\bar{+}\rangle \quad (\text{C2})$$

$$= \sum_{n=-\infty}^{\infty} \frac{1}{\sqrt{\pi\kappa\delta}} \int dv \int du e^{\frac{iuv}{2}} e^{-\frac{(u-u')^2}{2\delta^2}} e^{-iu(2n\sqrt{\pi}+v)} \times \exp\left(-\frac{(v-v')^2}{2\kappa^2}\right) \hat{Z}(2n\sqrt{\pi}+v) |p=0\rangle \quad (\text{C3})$$

We have

$$|\tilde{\psi}\rangle = \sum_{n=-\infty}^{\infty} \frac{\sqrt{2\pi\delta^2}}{\sqrt{\pi\kappa\delta}} \int dv \int du \frac{e^{-\frac{(u-u')^2}{2\delta^2}}}{\sqrt{2\pi\delta^2}} \times e^{-iu(2n\sqrt{\pi}+v/2)} e^{-\frac{(v-v')^2}{2\kappa^2}} \hat{Z}(2n\sqrt{\pi}+v) |p=0\rangle \quad (\text{C4})$$

$$= \sqrt{\frac{2\delta}{\kappa}} \sum_n \int dv e^{-\frac{(2n\sqrt{\pi}+v/2)^2}{2\delta^2}} e^{-iu'(2n\sqrt{\pi}+v/2)} \times e^{-\frac{(v-v')^2}{2\kappa^2}} \hat{Z}(2n\sqrt{\pi}+v) |p=0\rangle \quad (\text{C5})$$

$$= \sqrt{\frac{2\delta}{\kappa}} \sum_n e^{-\frac{(2n\sqrt{\pi}+v'/2)^2}{2\left(\frac{4+\delta^2\kappa^2}{4\delta^2}\right)}} \int dv e^{-\frac{\left(v+\frac{2\delta^2\kappa^2 2n\sqrt{\pi}-4v'}{4+\delta^2\kappa^2}\right)^2}{2\left(\frac{4\kappa^2}{4+\delta^2\kappa^2}\right)}} \times e^{-iu'(2n\sqrt{\pi}+v/2)} \hat{Z}(2n\sqrt{\pi}+v) |p=0\rangle \quad (\text{C6})$$

$$= \sqrt{2\pi} \sum_n \frac{e^{-\frac{(2n\sqrt{\pi}+v'/2)^2}{2\left(\frac{4+\delta^2\kappa^2}{4\delta^2}\right)}}}{\left(\pi\left(\frac{4+\delta^2\kappa^2}{4\delta^2}\right)\right)^{1/4}} \int dv \frac{e^{-\frac{\left(v+\frac{2\delta^2\kappa^2 2n\sqrt{\pi}-4v'}{4+\delta^2\kappa^2}\right)^2}{2\left(\frac{4\kappa^2}{4+\delta^2\kappa^2}\right)}}}{\left(\pi\left(\frac{4\kappa^2}{4+\delta^2\kappa^2}\right)\right)^{1/4}} \times e^{-iu'(2n\sqrt{\pi}+v/2)} \hat{Z}(2n\sqrt{\pi}+v) |p=0\rangle. \quad (\text{C7})$$

In the limit $\kappa^2\delta^2 \rightarrow 0$, we get

$$|\tilde{\psi}\rangle = \sqrt{2\pi} \sum_n \frac{e^{-\frac{\delta^2(2n\sqrt{\pi}+v'/2)^2}{2}}}{(\pi/\delta^2)^{1/4}} \int dv \frac{e^{-\frac{(v-v')^2}{2\kappa^2}}}{(\pi\kappa^2)^{1/4}} \times e^{-iu'(2n\sqrt{\pi}+v/2)} \hat{Z}(2n\sqrt{\pi}+v) |p=0\rangle. \quad (\text{C8})$$

The p -quadrature wavefunction of the above state $|\tilde{\psi}\rangle$ is given by

$$\langle p|\tilde{\psi}\rangle = \sqrt{2\pi} \sum_n \frac{e^{-\frac{\delta^2(2n\sqrt{\pi}+v'/2)^2}{2}}}{(\pi/\delta^2)^{1/4}} \int dv \frac{e^{-\frac{(v-v')^2}{2\kappa^2}}}{(\pi\kappa^2)^{1/4}} \times e^{-iu'(2n\sqrt{\pi}+v/2)} \delta(v - (p - 2n\sqrt{\pi})) \quad (\text{C9})$$

$$= \sqrt{2\pi} \sum_n \frac{e^{-\frac{\delta^2(2n\sqrt{\pi}+v'/2)^2}{2}}}{(\pi/\delta^2)^{1/4}} \frac{e^{-\frac{(p-2n\sqrt{\pi}-v')^2}{2\kappa^2}}}{(\pi\kappa^2)^{1/4}} \times e^{-i\frac{u'}{2}(p+2n\sqrt{\pi})}. \quad (\text{C10})$$

When $v' = \sqrt{\pi}$, the state has its support flipped to that of the ideal GKP qubit state $|\bar{-}\rangle$, however, with an envelope that is still only $\sqrt{\pi}/2$ shifted from the center of the envelope corresponding to the initial $|\bar{+}\rangle$ state. Thus, it is not quite $|\bar{-}\rangle$. The p -quadrature wavefunction description of the state is shown in Fig. 3.

-
- [1] Sergei Slussarenko and Geoff J. Pryde. Photonic quantum information processing: A concise review. *Applied Physics Reviews*, 6(4):041303, 2019.
 - [2] Fulvio Flamini, Nicolò Spagnolo, and Fabio Sciarrino. Photonic quantum information processing: a review. *Reports on Progress in Physics*, 82(1):016001, nov 2018.
 - [3] Jeremy L O’Brien, Akira Furusawa, and Jelena Vučković. Photonic quantum technologies. *Nature Photonics*, 3(12):687–695, 2009.
 - [4] Rafael N. Alexander, Shota Yokoyama, Akira Furusawa, and Nicolas C. Menicucci. Universal quantum computation with temporal-mode bilayer square lattices. *Phys. Rev. A*, 97:032302, Mar 2018.
 - [5] Shuntaro Takeda and Akira Furusawa. Universal quantum computing with measurement-induced continuous-variable gate sequence in a loop-based architecture. *Phys. Rev. Lett.*, 119:120504, Sep 2017.
 - [6] Nicolas C. Menicucci. Fault-tolerant measurement-based quantum computing with continuous-variable cluster states. *Phys. Rev. Lett.*, 112:120504, Mar 2014.
 - [7] Terry Rudolph. Why i am optimistic about the silicon-photonics route to quantum computing. *APL Photonics*, 2(3):030901, 2017.
 - [8] V. D. Vaidya, B. Morrison, L. G. Helt, R. Shahrokhshahi, D. H. Mahler, M. J. Collins, K. Tan, J. Lavoie, A. Reisinger, M. Menotti, N. Quesada, R. C. Pooser, A. E.

- Lita, T. Gerrits, S. W. Nam, and Z. Vernon. Broad-band quadrature-squeezed vacuum and nonclassical photon number correlations from a nanophotonic device. *Science Advances*, 6(39), 2020.
- [9] Warit Asavanant, Yu Shiozawa, Shota Yokoyama, Baramée Charoensombutamon, Hiroki Emura, Rafael N. Alexander, Shuntaro Takeda, Jun-ichi Yoshikawa, Nicolas C. Menicucci, Hidehiro Yonezawa, and Akira Furusawa. Generation of time-domain-multiplexed two-dimensional cluster state. *Science*, 366(6463):373–376, 2019.
- [10] Moran Chen, Nicolas C. Menicucci, and Olivier Pfister. Experimental realization of multipartite entanglement of 60 modes of a quantum optical frequency comb. *Phys. Rev. Lett.*, 112:120505, Mar 2014.
- [11] Han-Sen Zhong, Hui Wang, Yu-Hao Deng, Ming-Cheng Chen, Li-Chao Peng, Yi-Han Luo, Jian Qin, Dian Wu, Xing Ding, Yi Hu, Peng Hu, Xiao-Yan Yang, Wei-Jun Zhang, Hao Li, Yuxuan Li, Xiao Jiang, Lin Gan, Guangwen Yang, Lixing You, Zhen Wang, Li Li, Nai-Le Liu, Chao-Yang Lu, and Jian-Wei Pan. Quantum computational advantage using photons. *Science*, 370(6523):1460–1463, December 2020.
- [12] Max Tillmann, Borivoje Dakić, René Heilmann, Stefan Nolte, Alexander Szameit, and Philip Walther. Experimental boson sampling. *Nature Photonics*, 7(7):540–544, 2013.
- [13] Nicolas Gisin and Rob Thew. Quantum communication. *Nature Photonics*, 1(3):165–171, 2007.
- [14] S Pirandola, B R Bardhan, T Gehring, C Weedbrook, and S Lloyd. Advances in photonic quantum sensing. *Nature Photonics*, 12(12):724–733, 2018.
- [15] Adetunmise C Dada, Jonathan Leach, Gerald S Buller, Miles J Padgett, and Erika Andersson. Experimental high-dimensional two-photon entanglement and violations of generalized Bell inequalities. *Nature Physics*, 7(9):677–680, 2011.
- [16] Manuel Erhard, Robert Fickler, Mario Krenn, and Anton Zeilinger. Twisted photons: new quantum perspectives in high dimensions. *Light: Science & Applications*, 7(3):17146, 2018.
- [17] Chaohan Cui, Kaushik P. Seshadreesan, Saikat Guha, and Linran Fan. High-dimensional frequency-encoded quantum information processing with passive photonics and time-resolving detection. *Phys. Rev. Lett.*, 124:190502, May 2020.
- [18] Joseph M. Lukens and Pavel Lougovski. Frequency-encoded photonic qubits for scalable quantum information processing. *Optica*, 4(1):8–16, Jan 2017.
- [19] Jonathan Roslund, Renné Medeiros de Araújo, Shifeng Jiang, Claude Fabre, and Nicolas Treps. Wavelength-multiplexed quantum networks with ultrafast frequency combs. *Nature Photonics*, 8(2):109–112, 2014.
- [20] Valentin Averchenko, Denis Sych, Gerhard Schunk, Ulrich Vogl, Christoph Marquardt, and Gerd Leuchs. Temporal shaping of single photons enabled by entanglement. *Phys. Rev. A*, 96:043822, Oct 2017.
- [21] B. Brecht, Dileep V. Reddy, C. Silberhorn, and M. G. Raymer. Photon temporal modes: A complete framework for quantum information science. *Phys. Rev. X*, 5:041017, Oct 2015.
- [22] Farid Samara, Anthony Martin, Claire Autebert, Maxim Karpov, Tobias J. Kippenberg, Hugo Zbinden, and Rob Thew. High-rate photon pairs and sequential time-bin entanglement with si3n4 microring resonators. *Opt. Express*, 27(14):19309–19318, Jul 2019.
- [23] Harishankar Jayakumar, Ana Predojević, Thomas Kauten, Tobias Huber, Glenn S Solomon, and Gregor Weihs. Time-bin entangled photons from a quantum dot. *Nature Communications*, 5(1):4251, 2014.
- [24] Christian Weedbrook, Stefano Pirandola, Raúl García-Patrón, Nicolas J. Cerf, Timothy C. Ralph, Jeffrey H. Shapiro, and Seth Lloyd. Gaussian quantum information. *Rev. Mod. Phys.*, 84:621–669, May 2012.
- [25] Jun-ichi Yoshikawa, Shota Yokoyama, Toshiyuki Kaji, Chanond Sornphiphatphong, Yu Shiozawa, Kenzo Makino, and Akira Furusawa. Invited article: Generation of one-million-mode continuous-variable cluster state by unlimited time-domain multiplexing. *APL Photonics*, 1(6):060801, 2016.
- [26] C R Myers and T C Ralph. Coherent state topological cluster state production. *New Journal of Physics*, 13(11):115015, nov 2011.
- [27] T. C. Ralph, A. Gilchrist, G. J. Milburn, W. J. Munro, and S. Glancy. Quantum computation with optical coherent states. *Phys. Rev. A*, 68:042319, Oct 2003.
- [28] J. Eisert, S. Scheel, and M. B. Plenio. Distilling gaussian states with gaussian operations is impossible. *Phys. Rev. Lett.*, 89:137903, Sep 2002.
- [29] Julien Niset, Jaromír Fiurášek, and Nicolas J. Cerf. No-go theorem for gaussian quantum error correction. *Phys. Rev. Lett.*, 102:120501, Mar 2009.
- [30] Seth Lloyd and Samuel L. Braunstein. Quantum computation over continuous variables. *Phys. Rev. Lett.*, 82:1784–1787, Feb 1999.
- [31] Daniel Gottesman, Alexei Kitaev, and John Preskill. Encoding a qubit in an oscillator. *Phys. Rev. A*, 64(1):012310, June 2001.
- [32] Victor V. Albert, Kyungjoo Noh, Kasper Duivenvoorden, Dylan J. Young, R. T. Brierley, Philip Reinhold, Christophe Vuillot, Linshu Li, Chao Shen, S. M. Girvin, Barbara M. Terhal, and Liang Jiang. Performance and structure of single-mode bosonic codes. *Phys. Rev. A*, 97:032346, Mar 2018.
- [33] Kyungjoo Noh, Victor V Albert, and Liang Jiang. Quantum capacity bounds of gaussian thermal loss channels and achievable rates with Gottesman-Kitaev-Preskill codes, 2019.
- [34] Kosuke Fukui, Rafael N Alexander, and Peter van Loock. All-Optical Long-Distance quantum communication with Gottesman-Kitaev-Preskill qubits. November 2020.
- [35] Filip Rozpędek, Kyungjoo Noh, Qian Xu, Saikat Guha, and Liang Jiang. Quantum repeaters based on concatenated bosonic and discrete-variable quantum codes. November 2020.
- [36] Nicolas C. Menicucci, Peter van Loock, Mile Gu, Christian Weedbrook, Timothy C. Ralph, and Michael A. Nielsen. Universal quantum computation with continuous-variable cluster states. *Phys. Rev. Lett.*, 97:110501, Sep 2006.
- [37] P Campagne-Ibarcq, A Eickbusch, S Touzard, E Zalts-Geller, N E Frattini, V V Sivak, P Reinhold, S Puri, S Shankar, R J Schoelkopf, L Frunzio, M Mirrahimi, and M H Devoret. Quantum error correction of a qubit encoded in grid states of an oscillator. *Nature*, 584(7821):368–372, 2020.
- [38] Brennan de Neeve, Thanh Long Nguyen, Tanja Behrle, and Jonathan Home. Error correction of a logical grid

- state qubit by dissipative pumping. October 2020.
- [39] C Flühmann, T L Nguyen, M Marinelli, V Negnevitsky, K Mehta, and J P Home. Encoding a qubit in a trapped-ion mechanical oscillator. *Nature*, 566(7745):513–517, February 2019.
 - [40] K R Motes, B Q Baragiola, A Gilchrist, and N C Menicucci. Encoding qubits into oscillators with atomic ensembles and squeezed light. *Phys. Rev. A*, 2017.
 - [41] B. M. Terhal and D. Weigand. Encoding a qubit into a cavity mode in circuit qed using phase estimation. *Phys. Rev. A*, 93:012315, Jan 2016.
 - [42] Mihir Pant, Hari Krovi, Dirk Englund, and Saikat Guha. Rate-distance tradeoff and resource costs for all-optical quantum repeaters. *Phys. Rev. A*, 95:012304, Jan 2017.
 - [43] Kosuke Fukui, Akihisa Tomita, Atsushi Okamoto, and Keisuke Fujii. High-Threshold Fault-Tolerant quantum computation with analog quantum error correction. *Physical Review X*, 8(2), 2018.
 - [44] Yang Wang. Quantum error correction with the GKP code and concatenation with stabilizer codes. July 2019.
 - [45] A M Steane. Active stabilization, quantum computation, and quantum state synthesis. *Phys. Rev. Lett.*, 78(11):2252–2255, March 1997.
 - [46] Takaya Matsuura, Hayata Yamasaki, and Masato Koashi. Equivalence of approximate Gottesman-Kitaev-Preskill codes. October 2019.
 - [47] S Glancy and E Knill. Error analysis for encoding a qubit in an oscillator. *Phys. Rev. A*, 73(1):012325, January 2006.
 - [48] Michael Varnava, Daniel E. Browne, and Terry Rudolph. Loss tolerance in one-way quantum computation via counterfactual error correction. *Phys. Rev. Lett.*, 97:120501, Sep 2006.
 - [49] Ashlesha Patil. Stabilizer rules for graph state manipulations using fusion operations. in preparation.